Materials Horizons

ROYAL SOCIETY OF CHEMISTRY

REVIEW

View Article Online
View Journal

Cite this: DOI: 10.1039/d5mh02360b

Advanced polymeric membranes for CO_2 separation: fundamentals, materials, and practical challenges

Tae Hoon Lee, †[a] Byung Kwan Lee, †[b] Young Hoon Cho, [c] Hyo Won Kim, [d] Sang Hoon Han, [e] Seong Yong Ha [e] and Ho Bum Park *[b]

Received 10th December 2025,
Accepted 11th February 2026

DOI: 10.1039/d5mh02360b

rsc.li/materials-horizons

Membrane-based CO_2 separation is emerging as a central technology for achieving carbon neutrality, yet its widespread deployment remains constrained by longstanding trade-offs among permeability, selectivity, long-term stability, and scalability. This review provides the conceptual foundations, materials evolution, and market drivers shaping the next generation of polymeric CO_2 separation membranes. We first revisit the fundamentals of mass transport through dense polymer films and highlight how trade-offs arise from the interplay among solubility, diffusivity, and free-volume architecture. Building on this framework, we examine three major materials platforms that have redefined performance boundaries: thermally rearranged (TR) polymers that generate controlled microporosity through *in situ* cyclization; polymers of intrinsic microporosity (PIMs) that embody rigid, contorted backbones with permanent ultramicroporosity; and ether-rich CO_2-philic polymers that achieve high solubility selectivity and excellent processability. By integrating molecular-level insights with thin-film engineering considerations, we evaluate each material family's potential and limitations in realistic process environments. At the system level, we analyze global markets, including natural gas sweetening, post-combustion CO_2 capture, blue hydrogen purification, and biogas upgrading, where polymeric membranes are poised for rapid growth. Finally, we identify future research directions centered on stabilizing free volume, suppressing plasticization, enhancing thin-film robustness, and accelerating materials-to-module translation through digital design and advanced fabrication. Together, these strategies delineate a pathway for polymeric membranes to become scalable, energy-efficient tools for industrial CO_2 management in the coming decade.

Wider impact

Polymeric CO_2 separation membranes have the potential to become a scalable, energy-efficient pillar of industrial decarbonization, complementing and in some cases simplifying conventional absorption- and adsorption-based approaches. By connecting transport fundamentals with material evolution and realistic deployment constraints, this review clarifies why permeability–selectivity metrics must be interpreted alongside long-term stability, thin-film engineering, and manufacturability for real process environments. Our unified perspective on TR polymers, PIMs/ladder architectures, and ether-rich CO_2-philic polymers provides actionable design logic for tailoring membranes to application-specific demands spanning natural gas sweetening, post-combustion capture, blue hydrogen purification, and biogas upgrading. We also highlight how digital design, high-throughput evaluation, and closer academia–industry collaboration can shorten the path from record-setting materials to bankable modules, accelerating the adoption of membranes across CCUS value chains.

1. Introduction

The rapid accumulation of anthropogenic CO_2 in the atmosphere has become a defining constraint on the future of the global energy system. Meeting the temperature targets of the Paris Agreement and subsequent net-zero pledges requires not only the decarbonization of power generation, but also deep reductions in emissions from so-called "hard-to-abate" sectors

[a] *Department of Future Energy Engineering, Sungkyunkwan University, Suwon 16419, Republic of Korea*
[b] *Department of Energy Engineering, Hanyang University, Seoul 04763, Republic of Korea. E-mail: badtzhb@hanyang.ac.kr*
[c] *Separation and Purification Research Center, Chemical & Process Technology Division, Korea Research Institute of Chemical Technology, 141 Gajeong-ro, Yuseong-gu, Daejeon 34114, Republic of Korea*
[d] *Department of Energy Engineering, Korea Institute of Energy Technology (KENTECH), Naju 58330, Republic of Korea*
[e] *Airrane Co. Ltd, Cheongju 28121, Republic of Korea*
† These authors equally contributed to this work.

such as cement, steel, refining, and chemicals.[1,2] In virtually all credible mitigation scenarios, carbon capture, utilization, and storage (CCUS) plays a central role in bridging the gap between current infrastructure and a net-zero energy system. Within CCUS value chains, efficient and scalable gas separation technologies are indispensable for isolating CO_2 from diverse process streams and for conditioning hydrogen, syngas, and hydrocarbon feeds.[2,3]

Conventional CO_2 separation technologies, including chemical absorption using aqueous amines, cryogenic distillation, and pressure- or temperature-swing adsorption, are technologically mature and widely deployed.[2,4] However, they are energy-intensive, capital-intensive, and often difficult to downscale. Chemical absorption entails high thermal duty for solvent regeneration and significant solvent management issues.[5] Cryogenic processes deliver high purities but require deep cooling and substantial recompression, making them economically attractive only at large scale.[6] Adsorption-based systems offer flexibility in feed composition and operating pressure, yet they require complex multi-bed operation, are sensitive to contaminants, and can struggle with footprint and controllability in retrofit contexts.[7] As decarbonization expands from a small number of very large plants to a heterogeneous landscape of mid-scale and distributed emitters, there is an increasing need for compact, modular, and energy-efficient alternatives.

Polymeric membranes have emerged as a compelling candidate technology to address this need.[8] Membrane-based separations operate isothermally and without phase change, have no moving parts in the separation unit itself, and can be readily implemented in modular, skid-mounted systems.[8,9] Over the past four decades, polymeric membranes have been successfully commercialized for natural gas sweetening, hydrogen recovery in refineries, and nitrogen generation from air.[8,10–12] These deployments have validated the robustness and scalability of hollow-fiber and spiral-wound modules under industrial conditions. At the same time, advances in polymer chemistry and mixed-matrix architectures have pushed intrinsic permeability–selectivity performance beyond classical trade-off limits, suggesting the possibility of membranes tailored specifically for post-combustion CO_2 capture, biogas upgrading, and blue hydrogen production.[8]

In the context of CO_2 separation, membrane performance is governed primarily by the solution–diffusion mechanism.[11] Gas molecules dissolve into the polymer matrix at the high-pressure side, diffuse through free-volume elements under a chemical potential gradient, and desorb at the low-pressure side. The intrinsic material property that characterizes this behavior is the gas permeability, typically measured on dense films and expressed in Barrer (1 Barrer = 1×10^{-10} cm^3 (STP) cm cm^{-2} s^{-1} cm_{Hg}^{-1}). For practical membrane modules, however, the relevant figure of merit is gas permeance, expressed in GPU (1 GPU = 1×10^{-6} cm^3 (STP) cm^{-2} s^{-1} cm_{Hg}^{-1}), which reflects both intrinsic permeability and the thickness of the selective layer. Economically relevant process modeling studies suggest that for post-combustion capture, membranes must

Tae Hoon Lee

Dr Tae Hoon Lee is an Assistant Professor at Sungkyunkwan University (SKKU). After earning his PhD from Hanyang University in 2021 and conducting postdoctoral research at Massachusetts Institute of Technology (MIT), he joined the SKKU faculty in 2025. His research group focuses on designing advanced microporous materials for energy and environmental applications. Also, recognized with the 2025 NAMS Young Membrane Scientist Award, Dr Lee is dedicated to developing next-generation membranes for gas, liquid, and electrochemical systems.

Byung Kwan Lee

Byung Kwan Lee is a student in the integrated MS–PhD program at Hanyang University. His research interests focus on membrane-based gas and molecular separation using porous materials such as metal–organic frameworks (MOFs) and polymers of intrinsic microporosity (PIMs). He is also investigating the knowledge gap between the properties of PIMs in bulk films and thin-film membranes.

Ho Bum Park

Dr Ho Bum Park is a Professor and Chair of the Department of Energy Engineering at Hanyang University (HYU). Following his PhD at HYU (2002) and postdoctoral training at the University of Texas at Austin, he joined the HYU faculty in 2008. His research group focuses on developing advanced membrane materials for gas separation, liquid separation, and fuel cells. With over 230 SCI papers and 90 patents, Dr Park has made significant contributions to the field. He also provides extensive leadership in the academic community, including 18 years of service on the Membrane Society of Korea Board of Directors.

achieve CO_2 permeance in the range of ~1000 GPU or higher with CO_2/N_2 selectivity above ~30 to be competitive with advanced solvent systems in certain operating windows.[12,13]

Decades of work on dense films have established empirical "upper bounds" that quantify the trade-off between permeability and selectivity for a given gas pair.[14–16] Several key milestones in developing CO_2 separation membranes are summarized in Fig. 1. Early commercial materials such as cellulose acetate (CA) and polysulfone (PSf) defined the 1991 upper bound for CO_2/CH_4 separation, offering moderate selectivity at relatively low permeability.[8] The introduction of aromatic polyimides and related ultra-glassy polymers in the 1980s and 1990s shifted this limit upward by combining rigid backbones with moderate free volume. More recently, high-free-volume materials such as thermally rearranged (TR) polymers and polymers of intrinsic microporosity (PIMs) have pushed the 2008[14] and 2019[15] upper bounds substantially higher, demonstrating that simultaneously high permeability and selectivity is achievable through careful control of chain rigidity, contortion, and microporosity.[17,18]

Despite these advances, there remains a persistent and important gap between intrinsic material performance and module-level performance. Most upper-bound data are measured on dense films tens of micrometers thick, whereas practical gas separation modules rely on sub-micrometer selective layers fabricated as thin-film composites (TFCs) or integrally skinned asymmetric (ISA) hollow fibers.[19] When high-performance polymers are translated into these architectures, their permeance and selectivity frequently deviate from values predicted by simple thickness scaling. Plasticization under high CO_2 partial pressures can increase chain mobility and erode selectivity; physical aging can densify high-free-volume matrices and reduce permeability over time; and interfacial defects or support limitations can introduce additional transport resistance not captured in dense-film measurements.[10,11] As a result, the record-setting permeability–selectivity combinations reported in the materials literature only partially propagate into real membrane modules.

From an application standpoint, the requirements placed on CO_2 separation membranes are highly dependent on CO_2 concentration.[8,10,11] In natural gas sweetening and biogas upgrading, membranes must handle high CO_2 concentration (up to ~45%, often with H_2S and heavy hydrocarbons) at elevated feed pressures, with CO_2/CH_4 selectivity and plasticization resistance as key metrics. Post-combustion capture from flue gas, by contrast, involves low CO_2 partial pressures (~10–15% CO_2 at near-ambient pressure), high relative humidity, and the presence of SO_x, NO_x, and particulates; here, high CO_2 permeance and tolerance to water and contaminants are critical.[13] Direct air capture (DAC) poses an even more demanding challenge, with CO_2 concentrations near 0.04%, stringent pressure-drop limitations, and strong economic pressure on capital cost and energy use.[20,21] Emerging hydrogen and syngas applications add further complexity: in blue hydrogen production, membranes are used for H_2 purification and CO_2 removal at high pressures and temperatures, while in electrochemical CO_2 conversion systems, membranes must manage CO_2/CO separations and humidity near electrochemical interfaces.[2,3] The representative feed gas compositions and environments corresponding to each CO_2 separation application are summarized in Table 1.

These diverse process environments have driven the development of three broad classes of high-performance polymeric membranes that form the core of this review: (i) thermally rearranged (TR) polymers derived from ortho-functionalized polyimides, which generate rigid polybenzoxazole and related structures with tunable microporosity; (ii) polymers of intrinsic microporosity (PIMs), including spirocyclic, triptycene, Tröger's base, and CANAL-type ladder polymers, which encode microporosity directly into rigid, contorted backbones; and (iii) CO_2-philic ether-rich polymers, particularly polyethylene oxide (PEO)-based and poly(1,3-dioxolane) (PDXLA)-type systems, which exploit strong ether–CO_2 interactions to achieve high solubility selectivity. Each family embodies a distinct design philosophy for manipulating the balance between diffusivity and solubility, as well as different strategies for mitigating plasticization and physical aging.

At the same time, the rapidly evolving business environment for gas separation membranes is increasingly shaping research priorities. The global market for gas separation membranes is projected to grow faster than gross domestic product (GDP) over the next decade, with especially strong momentum in CO_2 separations.[22] Polymeric hollow-fiber membrane modules based on polyimides and related polymers currently dominate commercial deployment in natural gas processing and

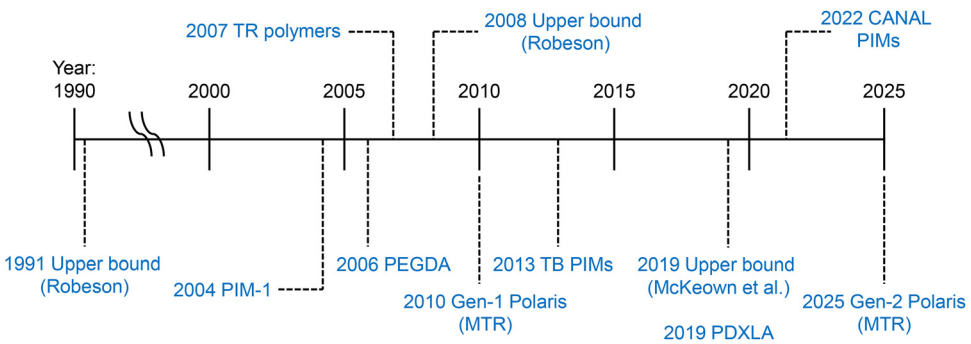

Fig. 1 Recent milestones in the development of polymeric membranes for CO_2 separation.

Table 1 Typical feed conditions for membrane-based CO_2 separation across major energy and environmental applications

CO_2 source/application	CO_2 concentration (%)	Key binary separation target	Pressure (bar)	Temperature (°C)	Relative humidity (%)
Pre-combustion CO_2 capture	15–40	CO_2/H_2	5–20	80–120	40–80
Natural gas purification	5–30 (up to 70 in sour gas)	CO_2/CH_4	20–60	20–50	0–10
Biogas upgrading	30–45	CO_2/CH_4	5–20	20–40	90–100
Post-combustion CO_2 capture	3–15	CO_2/N_2	~1	40–60	90–100
Direct air capture (DAC)	0.04	CO_2/N_2	~1	20–40	20–80
Syngas conditioning	5–30	CO_2/CO or CO_2/H_2	5–20	40–100	20–60
Electrochemical CO_2 conversion	5–40	CO_2/CO	1–5	20–60	40–90
Confined environments (*e.g.*, submarines and spacecraft)	0.5–2	CO_2/N_2 or CO_2/O_2	~1	20–25	40–70

hydrogen recovery, but there is growing interest in advanced materials and mixed-matrix membranes (MMMs) for higher-value separations and challenging feeds.[8] Membrane system integrators must align material choice not only with intrinsic performance metrics, but also with manufacturability, module cost, reliability, and compatibility with hybrid process configurations that combine membranes with absorption, adsorption, or cryogenics.

In this context, there is a need for a unified framework that connects fundamental transport principles, molecular-scale materials design, thin-film engineering, and market-driven application requirements. Previous reviews have often focused on either (i) material chemistry and Robeson-plot performance,[8,23] or (ii) techno-economic analyses and process design.[24,25] However, a comprehensive perspective that explicitly bridges the gap between dense-film transport properties, thin-film engineering, and real industrial opportunities remains relatively scarce.[9] For polymeric CO_2 separation membranes to move from record-setting laboratory demonstrations to bankable components of CCUS infrastructure, such an integrated view is essential.

Overall, the aim of this review is twofold. First, we provide a critical assessment of the state-of-the-art in polymeric membranes for CO_2 separation, emphasizing three major material families such as TR polymers, PIMs and related ladder architectures, and ether-rich CO_2-philic polymers, and highlighting how their molecular design governs transport, stability, and thin-film processability. Particular attention is given to the discrepancies between dense-film and thin-film performance, the roles of plasticization and physical aging in sub-micrometer layers, and the emerging strategies for stabilizing free volume and interfacial morphology. Second, we place these materials in the context of the evolving gas separation membrane market, identifying where (and under what conditions) advanced polymers are most likely to create value in CO_2 separations.

The article is organized as follows. Section 2 revisits the fundamentals of gas transport in polymeric membranes, including the solution–diffusion model, permeability–selectivity trade-offs, and the importance of membrane configuration and thin-film architecture. It also examines plasticization and physical aging as central constraints on long-term performance. Section 3 surveys the main classes of high-performance materials for CO_2 separation, TR polymers, PIMs, and ether-rich CO_2-philic systems, highlighting molecular design strategies, transport behavior, and stability in both dense and thin-film forms. Section 4 connects these materials to the current and emerging markets for gas separation membranes, discussing key application segments, regional trends, and the role of membranes within CCUS and hydrogen value chains. Finally, Section 5 outlines future directions and design principles, emphasizing materials–process co-design, thin-film engineering, and translational pathways needed to move polymeric CO_2 separation membranes from laboratory performance toward widespread industrial deployment.

2. Fundamentals of gas transport and performance limits in polymeric membranes for CO_2 separation

The performance of polymeric membranes for CO_2 separation is rooted in the molecular-scale processes that govern gas transport, the structural characteristics of the polymer matrix, and the architecture of the membrane itself. Although the solution–diffusion model has long served as the conceptual foundation of membrane science,[26] its implications become increasingly complex when high-performance polymers are translated from thick dense films into ultrathin selective layers used in industrial modules.[9] A rigorous understanding of these fundamentals—gas transport thermodynamics, the permeability–selectivity trade-off, and the dynamic phenomena of plasticization and physical aging—is essential for bridging the persistent gap between intrinsic material performance and real-world permeance.

The solution–diffusion model describes gas permeation as a sequence of sorption, diffusion, and desorption events. A gas molecule such as CO_2 first partitions into the polymer matrix according to its solubility, a thermodynamic quantity strongly influenced by polymer–penetrant interactions. CO_2, with its high condensability and pronounced quadrupole moment, exhibits strong affinity toward polar functionalities such as ether oxygens, carbonyls, amides, and nitriles. This interaction produces solubility coefficients far exceeding those of N_2 or CH_4, providing an immediate mechanism for enhancing CO_2 selectivity. Once sorbed, the molecule diffuses through the polymer by hopping between transient free-volume elements, a process dictated by the rigidity of the polymer backbone, packing efficiency, and the size of micropores. High-free-volume polymers such as TR polymers and PIMs facilitate rapid diffusion through interconnected pores in the sub-nanometer range, whereas conventional glassy polymers impose tighter diffusion constraints.

The overall permeability (P) of a gas is therefore the product of its diffusivity (D) and solubility (S), $P = D \times S$; materials that achieve outstanding permeability typically do so by optimizing one or both of these contributions. The solution-diffusion model also provides a conceptual basis for determining ideal selectivity, which is the ratio of permeabilities of two gases (A and B): $\alpha_{A/B} = P_A/P_B = (S_A/S_B) \times (D_A/D_B)$. This relationship shows that gas selectivity arises from two distinct contributions: solubility-selectivity, driven by thermodynamic interactions between polymer and gas, and diffusivity-selectivity, dictated by molecular size and free-volume characteristics of polymer. In general, CO_2/N_2 and CO_2/CH_4 separations benefit from both favorable solubility and moderate diffusivity selectivity,[8] whereas CO_2/H_2 separations often rely primarily on solubility effects due to the smaller kinetic diameter of hydrogen.[27]

However, in realistic gas mixtures, the actual separation performance often deviates from the ideal selectivity defined above.[8] In binary or mixed-gas systems, competitive sorption, plasticization, and coupled diffusion can alter gas transport behavior, leading to a practical performance parameter known as the separation factor $\left(\alpha'_{A/B}\right)$. The separation factor is defined as the ratio of the component concentration ratio in the permeate to that in the feed:

$$\alpha'_{A/B} = \frac{(y_A/y_B)}{(x_A/x_B)}$$

where y_A and y_B are the mole fractions of components A and B in the permeate, and x_A and x_B are those in the feed. This mixed-gas separation factor provides a more realistic measure of membrane performance under process-relevant conditions, as it captures the combined effects of gas–polymer interactions, concentration polarization, and multicomponent diffusion that are not reflected in single-gas-based ideal selectivity.[28,29]

Despite this mechanistic clarity, permeability alone is not a reliable indicator of practical performance. Dense-film permeability, typically measured using films tens of micrometers thick, reflects intrinsic transport phenomena but does not account for effects that arise when the polymer is processed into sub-micrometer selective layers, as found in thin-film composite (TFC) or integrally skinned asymmetric (ISA) membranes (Fig. 2).[19,30,31]

Dense (or thick) films

Dense, homogeneous polymer films represent the simplest configuration for fundamental transport studies and the initial screening of potential membrane materials. They are typically prepared as freestanding films with thicknesses of several tens of micrometers *via* slow solvent evaporation, which minimizes defects and enables accurate determination of intrinsic permeability and selectivity. Although such membranes are invaluable for understanding material properties, their extremely low permeance limits practical application, since gas permeance is inversely proportional to film thickness. Consequently, dense films are primarily used for laboratory-scale characterization and for establishing benchmark data on gas permeability and selectivity.

Integrally skinned asymmetric (ISA) membranes

To overcome the low permeance of dense films, integrally skinned asymmetric (ISA) membranes were developed, featuring a thin, dense skin layer on top of a porous substructure formed in a single step *via* phase inversion. Typical materials used for ISA membranes include PSf, CA, and polyimides. The thin skin layer serves as the selective barrier, while the porous substructure provides mechanical support with minimal mass-transfer resistance. This configuration significantly enhances permeance while maintaining gas selectivity, representing an important step toward scalable membrane modules. However, the formation of a uniform and defect-free skin layer is highly sensitive to fabrication parameters such as polymer concentration, solvent–nonsolvent exchange rate, and temperature, making process control critical for reproducibility and scale-up. Moreover, the applicability of the phase inversion process is restricted to polymers that are soluble in high-boiling polar aprotic solvents – such as *N*-methyl-2-pyrrolidone (NMP), *N*,*N*-dimethylacetamide (DMAc), or *N*,*N*-dimethylformamide (DMF) – and capable of forming stable asymmetric structures during coagulation. In addition, phase inversion typically requires large volumes of organic solvents and nonsolvent baths, resulting in significant solvent waste and environmental burden. It is also worth noting that, while only the ultrathin skin layer is responsible for the actual gas separation, the majority of the raw polymer material is consumed to form the porous substructure, leading to substantial material waste.[10,11]

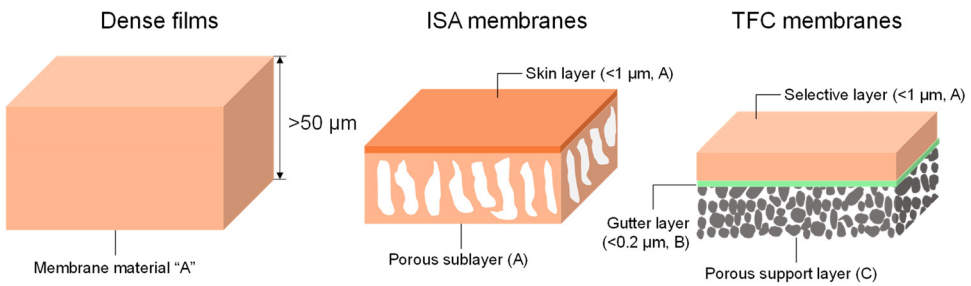

Fig. 2 Schematic illustration of three representative membrane configurations: a dense (or thick) film (left), an integrally skinned asymmetric (ISA) membrane (middle), and a thin-film composite (TFC) membrane consisting of an ultrathin selective layer supported by a porous substrate coated with a gutter layer (right).

Thin-film composite (TFC) membranes

The TFC architecture represents the most advanced configuration for modern gas separation. It typically consists of three layers: a porous support (commonly polyacrylonitrile (PAN) or PSf), a highly permeable gutter layer, and an ultrathin selective layer, typically less than 1 μm thick. The selective layer can be deposited by various techniques such as spin coating, bar coating, dip coating, interfacial polymerization, or molecular layer-by-layer assembly. The introduction of a high-permeability intermediate layer, often referred to as the gutter layer, minimizes mass-transfer resistance between the selective coating and the porous substrate, thereby preventing performance loss that occurs when the support becomes the dominant transport bottleneck. By integrating chemical tunability with scalable multilayer structures, TFC membranes combine the flexibility of polymer chemistry with the high gas flux required for industrial applications, achieving permeances one to two orders of magnitude higher than those of dense films.[10,11] Industrial membrane modules rely overwhelmingly on these architectures because they offer high permeance at minimal material cost. In such configurations, even minor variations in selective-layer thickness, substrate resistance, or interfacial morphology can substantially alter overall permeance. The presence of a gutter layer—often a highly permeable silicone-based coating—is essential to minimize resistance imposed by the porous support. When the gutter layer is insufficiently permeable, or when the selective coating infiltrates into the substrate pores, the effective permeance can fall far below the level predicted by simple thickness scaling from dense films.[32,33] This disparity, often termed the "knowledge gap" in membrane science, highlights the crucial distinction between intrinsic permeability and operational permeance.

One of the most important concepts in polymeric membrane science is the permeability–selectivity trade-off described by Robeson's upper bound.[14,34] Over decades of research, polymers have been observed to cluster along an empirical line in log–log space: materials with high permeability tend to exhibit low selectivity and *vice versa*. The molecular origin of this trade-off lies in the tension between free-volume expansion and size-sieving capability.[35] Increasing free volume generally enhances gas diffusivity, improving permeability, but simultaneously reduces the polymer's ability to discriminate between molecules of slightly different kinetic diameters. Conversely, reducing free volume sharpens molecular discrimination at the expense of permeability. Moving beyond this trade-off requires strategies that decouple free volume from selectivity—for example, through the introduction of rigid, contorted backbones that preserve microporosity without compromising structural integrity. Such design principles underlie the exceptional performance of TR polymers, spirocyclic and triptycene-based PIMs, Tröger's base polymers, and CANAL-type ladder polymers, which collectively shifted the upper bound upward in 2008[14] and again in 2019[15] (Fig. 3).

While the upper bound defines the landscape of intrinsic transport behavior, two dynamic phenomena—plasticization and physical aging—impose practical constraints, particularly in high-free-volume materials (Fig. 4). *Plasticization* arises when CO_2 sorption induces swelling of the polymer matrix, increasing segmental mobility and enlarging free volume. As a result, permeability increases while selectivity deteriorates, a particularly problematic outcome for high-pressure separations such as natural gas sweetening and hydrogen purification. Polymers experience a characteristic plasticization pressure beyond which transport properties deviate sharply from their single-gas measurements.[36] Mitigating plasticization requires restricting chain mobility through crosslinking, incorporating bulky or rigid segments, or using polymers whose architecture inherently resists CO_2-induced relaxation.

Physical aging presents a complementary challenge, especially for microporous glassy polymers in a thin-film form. Many high-performance polymers are synthesized in a nonequilibrium, high-free-volume state; over time, polymer chains relax toward a denser configuration, reducing free volume and decreasing permeability. This densification is significantly

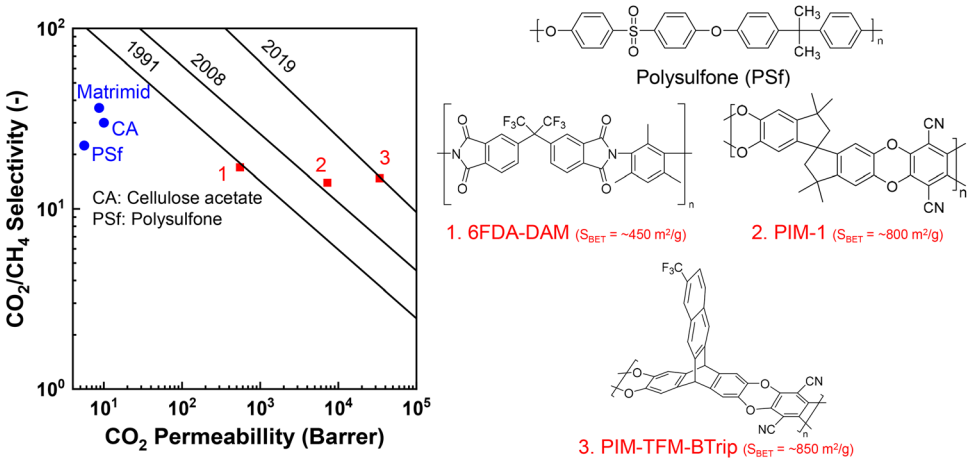

Fig. 3 Permeability–selectivity upper bounds for polymeric CO_2/CH_4 separation membranes reported in 1991,[34] 2008,[14] and 2019,[15] along with the chemical structures of a representative conventional polymer (PSf) and typical PIM materials. S_{BET} = Brunauer–Emmett–Teller (BET) surface area.

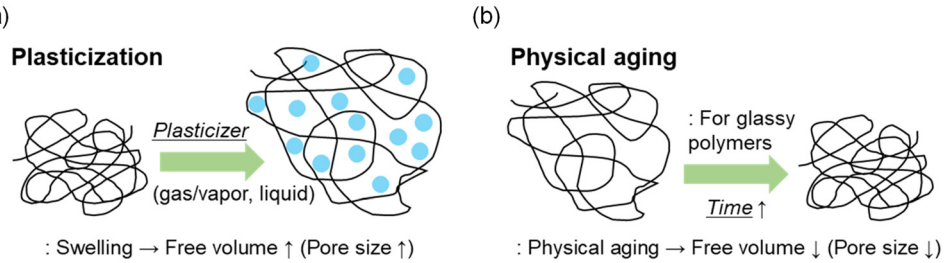

Fig. 4 Schematic illustrations of (a) plasticization and (b) physical aging challenges in polymeric membranes.

accelerated as film thickness decreases because surface mobility and free-volume collapse become more pronounced. PIMs, TR polymers, and other ultra-microporous systems are therefore particularly susceptible to rapid aging when processed into sub-100-nm films.[37] Stabilizing free volume through crosslinking, bulky building blocks, or post-synthetic modifications has proven essential for extending their operational viability.

Finally, the morphology of thin selective layers, often overlooked in dense-film-based studies, can dominate real membrane performance. The selective layer may undergo interdiffusion with the gutter layer or rigidification at the interface, altering gas transport pathways.[32,33] Coating defects, surface roughness, or rapid solvent evaporation can lead to nanoscale pinholes that compromise selectivity. Moreover, the effective resistance of the gutter layer can limit overall permeance even when the selective polymer itself exhibits outstanding intrinsic performance. These considerations underscore that membrane design is an inherently hierarchical challenge: material chemistry, thin-film structure, and module-level architecture are deeply interdependent.

Together, these fundamentals highlight the key physical principles that govern CO_2 separation using polymeric membranes. They explain why dense-film measurements alone cannot predict operational behavior, why upper-bound performance requires translation into stable thin films, and why plasticization and aging remain central obstacles in deploying high-free-volume polymers. They also frame the constraints and opportunities that guide the development of advanced materials discussed in Section 3. By integrating transport theory with thin-film engineering and stability considerations, researchers can more effectively design polymers that not only achieve exceptional intrinsic performance but also maintain durability and manufacturability in realistic separation environments.

3. Materials for high-performance CO_2 separation

3.1. Thermally rearranged (TR) polymers

Thermally rearranged (TR) polymers represent one of the most influential breakthroughs in the design of polymeric membranes for CO_2 separation.[17,38] Their emergence fundamentally altered the prevailing understanding of how high permeability and high selectivity could be simultaneously achieved, challenging the long-established permeability–selectivity trade-off. TR polymers are uniquely defined by their post-synthetic transformation: they originate from well-defined aromatic polyimide precursors containing *ortho*-hydroxyl functionalities and are converted into highly rigid polybenzoxazole (PBO) or polybenzimidazole (PBI) structures when heated to elevated temperatures, typically between 350 and 450 °C.[38,39] During this solid-state rearrangement process, the polymer undergoes intramolecular cyclization accompanied by decarboxylation, resulting in a dramatic increase in free volume and generation of a microporous, ladder-like backbone (Fig. 5a).[38]

The fundamental appeal of TR polymers lies in their capacity to combine extreme rigidity with permanent microporosity—two attributes that are often mutually exclusive in conventional glassy polymers. Thermal rearrangement triggers a structural reorganization that redefines the topology of free-volume elements within the material. Whereas typical polyimides possess tight packing with limited nanoporosity, their TR derivatives develop interconnected micropores in the 0.5–1.0 nm range, which are ideally suited for size-sieving mechanisms. Molecular simulations and positron annihilation lifetime spectroscopy (PALS) consistently reveal that the conversion process results not merely in an increase in fractional free volume (Fig. 5b),[38,40] but in a qualitative change in the pore size distribution: small voids coalesce into larger, more continuous cavities that provide efficient pathways for small, condensable gases such as CO_2.

A defining advantage of the TR approach is its circumvention of solubility limitations normally associated with ultra-rigid polymers. PBOs and PBIs, in their fully synthesized forms, are typically insoluble or only sparingly soluble in common solvents, making conventional solution processing extremely difficult. TR chemistry offers an elegant workaround: one can process the soluble and mechanically robust polyimide precursor into films or hollow fibers using well-established methods, and only then induce rearrangement through controlled thermal treatment.[38,41,42] This modularity allows researchers to finely tune the rearrangement temperature, duration, and atmosphere to achieve desired levels of conversion and microporosity. In this way, TR polymers permit systematic design of free volume, permeability, and mechanical properties through a single processing parameter (*i.e.*, thermal history).

The impact of TR polymers on CO_2 separation performance has been profound. Early work demonstrated that fully converted TR polymers based on 6FDA-HAB or analogous

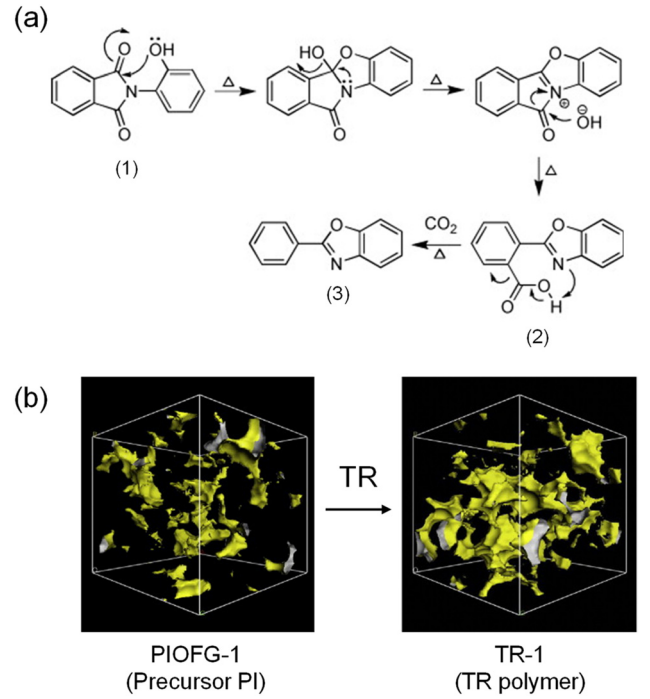

Fig. 5 (a) Schematic thermal rearrangement pathway from a hydroxyl-functionalized polyimide to a polybenzoxazole: (1) an imide ring with an ortho-hydroxyl group, (2) a carboxyl–benzoxazole intermediate, and (3) the resulting benzoxazole ring. (b) Simulated free-volume distribution of the PIOFG-1 and TR-1 polymers (yellow: accessible free volume, probe size = 1.1 Å).[38] Reproduced from ref. 38 with permission from Elsevier, copyright 2010.

precursors could achieve CO_2 permeability values surpassing those of nearly all conventional glassy polymers by an order of magnitude, while maintaining CO_2/CH_4 and CO_2/N_2 selectivities well above levels expected from their free volume.[38,43] This unusual combination, high permeability without a corresponding collapse in selectivity, positioned TR polymers above the 2008 Robeson upper bound and influenced the development of later microporous polymer families (Fig. 6).[17] Mechanistically, TR polymers exhibit high diffusivity for CO_2 due to their expanded microporous network, but the rigid benzoxazole linkages restrict larger penetrants through steric effects, preserving size-sieving capability. In essence, TR polymers achieve what most polymer membranes struggle to balance: high CO_2 diffusivity without sacrificing diffusivity selectivity.

An equally important dimension of TR polymer development pertains to their mechanical and chemical robustness. The benzoxazole-linked backbones produced through rearrangement possess exceptional thermal stability, solvent resistance, and stiffness.[39,44] These properties enable TR membranes to withstand aggressive high-pressure CO_2 environments commonly encountered in natural gas purification or hydrogen production. Many polyimides undergo significant plasticization under elevated CO_2 pressures due to increased chain mobility; by contrast, TR polymers exhibit a markedly delayed or even suppressed plasticization response.[17] Crosslinking strategies implemented either before or after rearrangement further suppress CO_2-induced swelling by restricting segmental motion. These stability advantages have made TR polymers strong candidates for industrially relevant gas separations, where predictable performance over extended timeframes is crucial.[42]

Despite their impressive dense-film performance, the translation of TR polymers into practical thin-film or hollow-fiber forms initially proved challenging. Fully rearranged TR films are typically brittle and prone to cracking due to the extreme rigidity of the benzoxazole network. This brittleness complicates fabrication of defect-free coatings below 1 μm—an essential requirement for high-permeance membranes. Early efforts to deposit TR polymers as selective layers on porous supports often resulted in pinholes, delamination, or poor adhesion.[45,46]

To overcome these obstacles, several molecular engineering strategies were developed. One approach involves introducing bulky or flexible substituents into the polyimide precursor to relieve internal stresses during rearrangement.[38,39,43,47] Incorporating units such as spirobisindane, triptycene, or kinked aromatic linkages provides controlled contortion without compromising the structural integrity of the rearranged polymer.[48,49] These modifications yield TR films with enhanced ductility and improved coating behavior while retaining high permeability and selectivity.

Another notable advancement lies in the integration of TR polymers into hollow-fiber architectures (Fig. 7).[42] Hollow fibers represent the most industrially scalable membrane configuration owing to their high packing density and mechanical resilience. However, producing hollow fibers from ultra-rigid materials is nontrivial. Crosslinking-assisted densification strategies have proven effective in producing TR-based hollow fibers capable of withstanding high feed pressures without collapsing. These fibers exhibit high CO_2 permeance and stable CO_2/N_2 selectivity, bridging the long-standing gap between intrinsic TR polymer performance and practical module-level implementation.

Beyond structural challenges, the thin-film performance of TR polymers highlights their inherent advantages in resisting physical aging. Whereas many high-free-volume polymers, especially early-generation PIMs, experience rapid densification and permeability loss in thin-film form, TR polymers exhibit relatively mild aging behavior.[50] Their rigid aromatic frameworks resist large-scale rearrangements, and the microporous architecture generated during thermal rearrangement remains remarkably stable over time. This stability is especially valuable in thin layers where high surface-to-volume ratios typically accelerate aging.

The conceptual significance of TR polymers extends even further. Their emergence demonstrated that permanent microporosity and high chain rigidity can be engineered *via* post-synthetic transformation rather than being encoded entirely in the monomer structure. This opened the door to a new paradigm in polymer design: microporosity generated *in situ* after casting, rather than through specialized monomers or multi-step ladder polymerization routes.[51] The success of TR polymers has directly inspired several modern high-performance polymer families, including advanced PIMs, contorted ladder polymers,

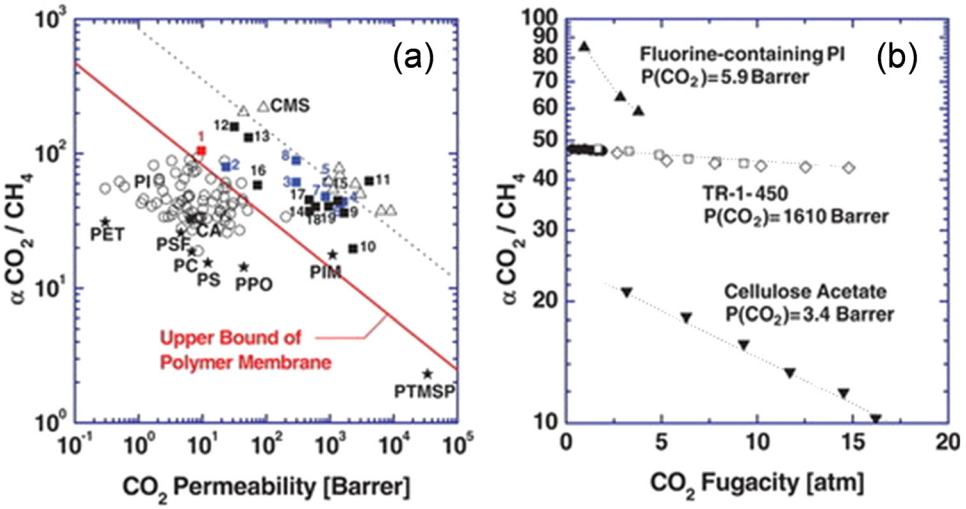

Fig. 6 (a) The plot compares CO_2 permeability and CO_2/CH_4 selectivity for a series of TR polymers, including PIOFG-1 and multiple TR-1 derivatives prepared under different thermal or doping conditions. All TR polymer data points were obtained from pure-gas measurements at 35 °C. For context, permeability–selectivity values of conventional polyimides and other common membrane polymers reported in the literature are also shown. The Robeson upper bound is indicated, with a dotted line serving as a visual guide. (b) The influence of CO_2 partial pressure on mixed-gas CO_2/CH_4 selectivity for TR-1-450 at 35 °C, evaluated at feed ratios of 10 : 90, 50 : 50, and 80 : 20 (CO_2 : CH_4). Mixed-gas data for a fluorine-containing polyimide and cellulose acetate, along with their CO_2 permeabilities measured at 10 atm and 35 °C, are included for comparison, and dotted lines are provided as guides to the eye.[17] Reproduced from ref. 17 with permission from The American Association for the Advancement of Science, copyright 2007.

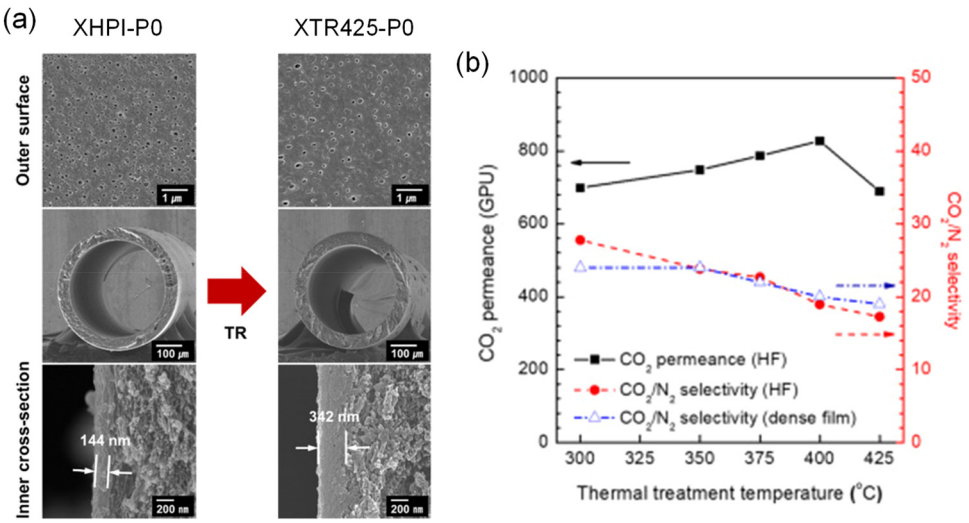

Fig. 7 (a) SEM images of XHPI-P0 (precursor PI) hollow fibers and XTR425-P0 (TR polymer) fibers after thermal treatment, highlighting changes in the outer surface and lumen-side cross-section. (b) CO_2 permeance (black solid line) and CO_2/N_2 selectivity (red dashed line) of XTR hollow fibers, with the blue dash-dot line representing the ideal CO_2/N_2 selectivity of the corresponding dense XTR film.[42] Reproduced from ref. 42 with permission from Elsevier, copyright 2019.

Tröger's base architectures, and CANAL-type materials that further extend the boundaries of free-volume engineering.

In summary, TR polymers represent a foundational class of high-performance materials for CO_2 separation. Their unique combination of tunable microporosity, exceptional thermal and chemical stability, resistance to plasticization, and compatibility with scalable processing techniques positions them as one of the most mature and industrially relevant families among next-generation gas separation polymers. They serve as a bridge between conventional polyimides and ultrahigh-free-volume ladder polymers, demonstrating that carefully orchestrated post-synthetic transformations can fundamentally reshape membrane performance. The principles established through TR polymer research—rigidity, micropore formation, tunability, and mechanical stabilization—provide an essential framework for understanding the more diverse and structurally complex families of polymers discussed in the following sections.

3.2. Polymers of intrinsic microporosity (PIMs)

Polymers of intrinsic microporosity (PIMs) represent one of the most transformative advances in polymer membrane science over the past two decades.[18] Unlike conventional glassy polymers, in which microporosity arises as a secondary consequence of inefficient packing, PIMs embed microporosity directly into their molecular architecture through rigid, contorted, ladder-like structures (Fig. 8).[52] In doing so, they provide a powerful and conceptually distinct strategy for achieving extremely high gas permeability without compromising selectivity. Their emergence has reshaped the Robeson upper bound,[14–16] redefined structure–property relationships for gas transport, and provided a versatile platform for designing tailored functionalities, enhanced stability, and mixed-matrix systems.

The defining characteristic of PIMs is intrinsic microporosity—nanopores formed not as a result of post-processing or thermal rearrangement, but as a direct consequence of a backbone that cannot pack efficiently.[18] Most PIMs incorporate rigid ladder or semi-ladder structures with contorted monomers—such as spirocenters, triptycene units, or sterically frustrated linkages—that enforce three-dimensional geometric constraints preventing close chain packing. As a result, PIMs possess interconnected free volume elements typically in the 0.4–0.8 nm range, ideally suited for rapid diffusion of small gas molecules. This design leads to permeabilities often exceeding 1000 Barrer for CO_2, far surpassing those of conventional glassy polymers, while maintaining meaningful size-sieving behavior.

Early PIMs, particularly PIM-1 derived from a spirobisindane-based polymerization reaction (Fig. 9),[53] demonstrated that extremely high permeability could be achieved in solution-processable materials, challenging previous assumptions that ultrapermeable polymers would inevitably be mechanically fragile or insoluble. The solubility and excellent film-forming properties of PIM-1 enabled widespread characterization and rapid adoption across gas separation research, effectively catalyzing a new era of polymer design centered on intrinsic microporosity. However, despite their promising performance, first-generation PIMs also highlighted key challenges associated with high-free-volume polymers: rapid physical aging and significant susceptibility to CO_2-induced plasticization.[37,54,55] These limitations prompted extensive research into modified PIM architectures, functional group incorporation, ladder polymer diversification, and post-synthetic modifications designed to stabilize free volume.

Following the success of PIM-1, extensive efforts were made to expand the design library of solution-processable PIMs. The key strategy has been to modify the micropore-generating unit, maintaining rigidity while tuning chain connectivity and intersegmental angles. Among these developments, a notable advance was the introduction of spirobifluorene (SBF)-based PIMs (*i.e.*, PIM-SBF).[56] By replacing the spirobisindane moiety of PIM-1 with a more rigid spirobifluorene unit, the chain bending angle was preserved while rotational freedom around the spiro-center was further constrained (Fig. 10). This molecular design enhanced backbone rigidity and improved size-sieving ability without compromising processability. Gas permeation studies confirmed that PIM-SBF exhibits similar or slightly higher permeability than PIM-1 but with significantly improved selectivity for key gas pairs such as CO_2/CH_4, O_2/N_2, and H_2/N_2. The improvement stems primarily from enhanced diffusivity selectivity due to the tighter distribution of micropore dimensions, while the solubility selectivity remains comparable.

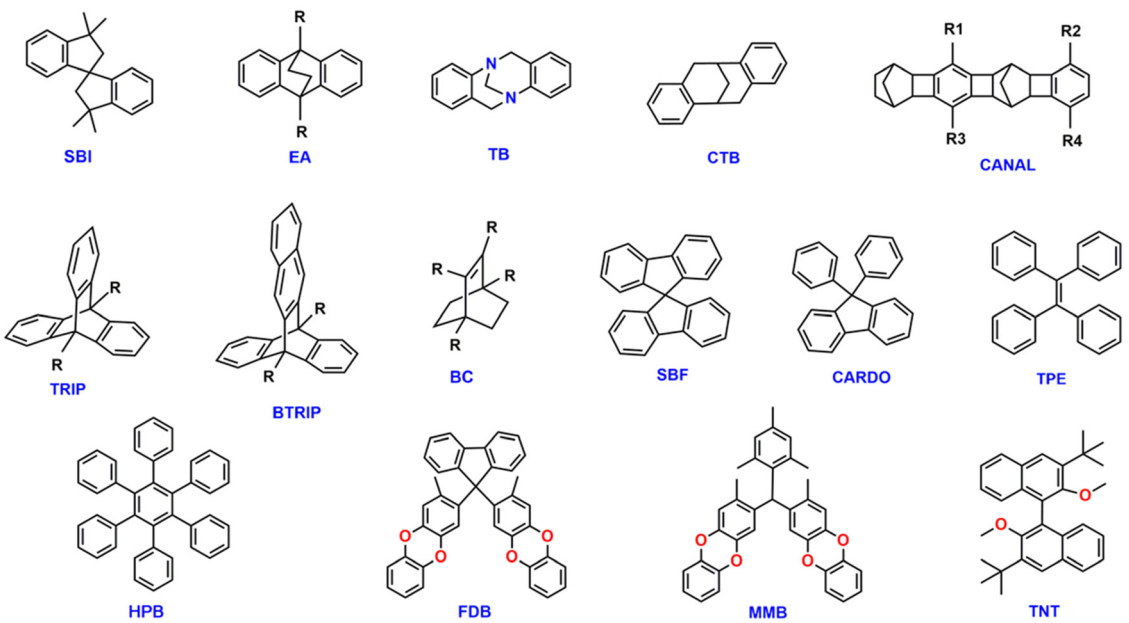

Fig. 8 Representative organic building blocks used in the design and synthesis of PIMs for membrane applications, including spirobisindane (SBI), phenazine, binaphthyl, spirobifluorene (SBF), hexaphenylbenzene (HPB), tetraphenylethylene (TPE), triptycene (TRIP), ethanoanthracene (EA), Tröger's base (TB), and norbornyl benzocyclobutene units derived from catalytic arene–norbornene annulation (CANAL).[52]

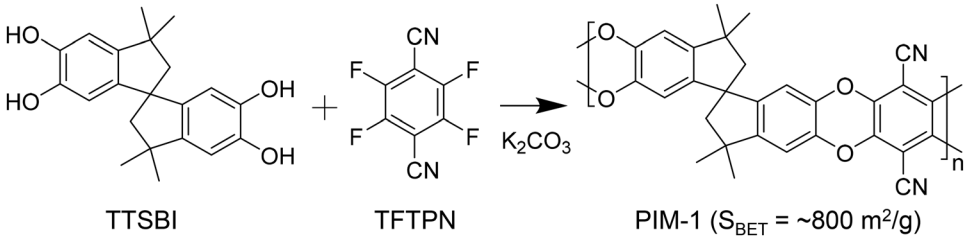

Fig. 9 Synthetic route and chemical structure of PIM-1. TTSBI = 3,3,3′,3′-tetramethyl-1,1′-spirobiindane-5,5′,6,6′-tetraol; TFTPN = tetrafluoroterephthalonitrile; S_{BET} = Brunauer–Emmett–Teller (BET) surface area.

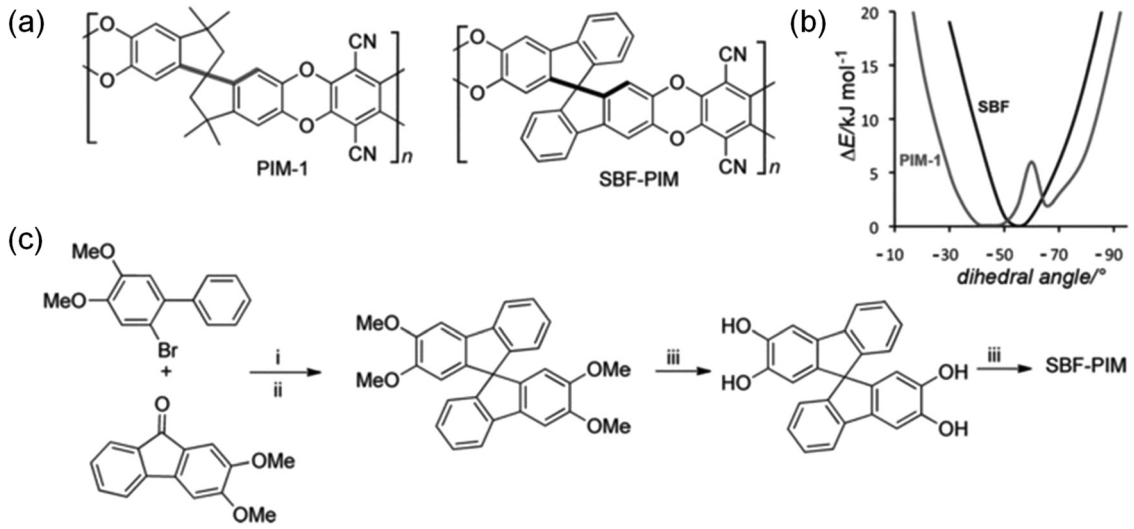

Fig. 10 (a) Chemical structures of PIM-1 and PIM-SBF. (b) Energy profiles as a function of dihedral-angle deviation around the spiro-center for PIM-1 and PIM-SBF, highlighting the increased chain rigidity of PIM-SBF. (c) Synthetic procedure for PIM-SBF. Conditions: (i) BuLi, THF/hexane, 12 h; (ii) HCl/AcOH, reflux 3 h, yield 75%; (iii) BBr_3, $CHCl_3$, 2 h, yield 92%; (iv) 2,3,5,6-tetrafluoroterephthalonitrile, K_2CO_3, DMF, 65 °C, 96 h, yield 86% after reprecipitation.[56] Reproduced from ref. 56 with permission from John Wiley and Sons, copyright 2012.

Consequently, PIM-SBF data points lie well above the 2008 Robeson upper bound, providing clear experimental validation of the long-standing hypothesis that increased polymer chain rigidity, coupled with preserved free volume, can simultaneously enhance permeability and selectivity.

Triptycene, another widely used building block, incorporates a rigid ''3D paddlewheel'' framework with inherent cavities.[57] These monomers create persistent, interconnected micropores, unlike flexible polymers, where free volume fluctuation must be thermally induced. The rigidity ensures that microporosity does not collapse easily, while the contortion prevents the formation of extended planar structures that would otherwise reduce porosity. At the same time, these monomeric motifs provide opportunities for tuning microporosity, as variations in steric bulk, connectivity, and ladder architecture influence pore size distribution and packing frustration.[57–59] The next major advance came from a systematic investigation of benzotriptycene-based PIMs, which established a quantitative relationship between micropore topology and gas transport performance.[60] These materials consistently exhibited CO_2 permeabilities exceeding 4000 Barrer with CO_2/N_2 selectivities above 30, outperforming nearly all previously reported solution-processable polymers. By analyzing multiple benzotriptycene derivatives, researchers proposed new upper bounds for both CO_2/N_2 and CO_2/CH_4 separations, effectively redefining the 2019 upper bound limits for polymeric membranes (Fig. 11).[15] These revised correlations reflect a steeper slope in Robeson-type plots, indicating that diffusivity and solubility selectivities can be simultaneously optimized through precise control of contorted aromatic packing. The outcome demonstrated that iptycene-based PIMs, when rationally engineered for hierarchical micropore distribution, can achieve permeability–selectivity combinations once thought unattainable for processable polymers.[61–63]

Beyond the classical PIM-1 structure, a diverse family of PIMs has emerged through incorporation of alternative rigid linkages, heteroatoms, and three-dimensional scaffolds. Tröger's base (TB) polymers (Fig. 12), for example, introduce a bicyclic nitrogen-containing bridge into the polymer chain, generating ultra-rigid structures with substantial contortion.[64–66] TB-PIMs exhibit exceptional microporosity, pushing CO_2 permeability toward 10 000 Barrer in some formulations, while still maintaining CO_2/CH_4 and CO_2/N_2 selectivities above the Robeson 2008 upper bound. Another important class is

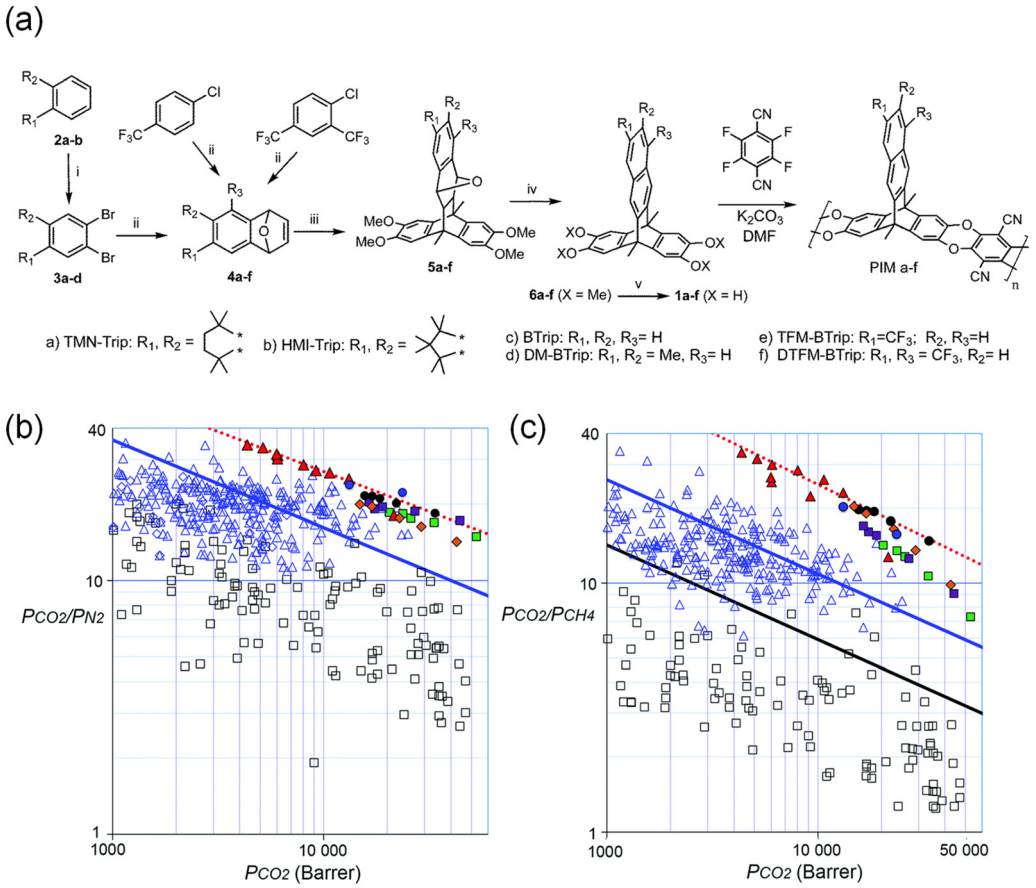

Fig. 11 (a) Structure and synthetic route of benzotriptycene-based PIMs. Reaction conditions: (i) Br_2, Fe, DCM, rt, 3 h; (ii) *n*-BuLi, furan, THF, −78 °C, 1.5 h; (iii) 9,10-dimethyl-2,3,6,7-tetramethoxyanthracene, DMF, 250 °C, 7 bar, microwave irradiation, 2 h; (iv) TFA or $MeSO_4H$, rt, 24 h; (v) BBr_3, DCM. (b) and (c) Robeson plots for (b) CO_2/N_2 and (c) CO_2/CH_4 separation, showing the gas-permeability performance of benzotriptycene-based PIM films. The proposed revised upper bounds for both gas pairs are indicated by red dashed lines.[15]

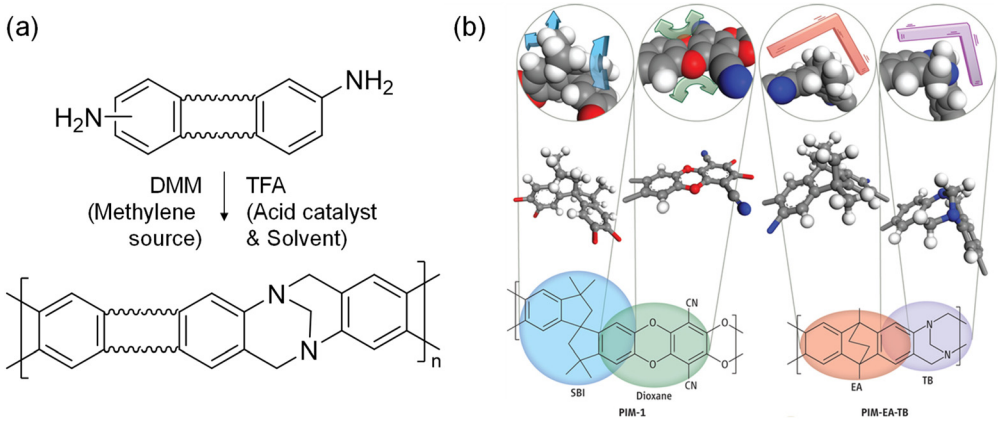

Fig. 12 (a) Synthetic scheme for Tröger's base (TB) polymers derived from aromatic diamines. (b) Microporous polymers with contorted ladder architectures resist rotational motion, enabling them to maintain a more uniform pore structure. PIM-1 incorporates SBI and dioxane linkages, both of which retain considerable conformational flexibility. In contrast, the PIM-EA-TB reported by Carta *et al.* features EA (ethanoanthracene) and TB units that create a significantly more rigid backbone. This enhanced rigidity yields high gas permeability while enabling precise size discrimination among gases with subtle differences in molecular dimensions.[66,67] Reproduced from ref. 67 with permission from The American Association for the Advancement of Science, copyright 2013.

benzotriptycene-based PIMs, which incorporate expanded 3D motifs that further amplify internal cavities and ultrasonically enhance diffusivity for condensable gases. Similarly, spirobisindane- and triptycene-containing ladder polymers have been

synthesized to achieve high molecular weight, excellent mechanical robustness, and tunable microporosity, while preserving the signature contortion responsible for high gas transport rates.[16,54,62,66]

CANAL polymers, synthesized by catalytic arene–norbornene annulation (CANAL) polymerization, represent one of the most advanced families within the PIM domain.[68,69] Their backbones are characterized by fused-ring, double-stranded architectures that are not only rigid but also extremely shape-persistent, preventing collapse under thermal or mechanical stress. CANAL polymers display some of the highest CO_2 permeabilities among solution-processable polymers, often above 5000 Barrer, while maintaining selectivities comparable to or surpassing those of earlier PIM analogs.[69] Their ladder structures restrict torsional freedom, resist physical aging, and create interconnected microporous networks with remarkable stability. These attributes have made CANAL systems a subject of significant interest in attempts to engineer PIM-inspired materials that translate high intrinsic performance into practical thin film membranes. Building on this foundation, more recent developments have introduced three-dimensional (3D) contorted hydrocarbon ladder polymers that further extend CANAL chemistry. By integrating fluorene or dihydrophenanthrene cores into the polymer backbone, the resulting networks adopt highly distorted 3D geometries that amplify both microporosity and size-sieving precision.[69] These hydrocarbon-based ladder polymers display an unusual combination of high selectivity and high permeability, surpassing many established upper-bound correlations for critical gas pairs such as CO_2/CH_4 and H_2/CH_4. Remarkably, unlike conventional PIMs that experience severe permeability decay upon aging, these 3D CANAL polymers exhibit beneficial aging effects: their selectivity increases over time while permeability remains largely preserved or even improved (Fig. 13).[69] Detailed transport analyses revealed that this enhancement arises from gradual narrowing of diffusion pathways that preferentially restrict larger gas molecules, effectively sharpening molecular sieving without diminishing overall flux.

Despite their exceptional intrinsic performance, PIMs face a fundamental challenge: physical aging. High-free-volume glassy polymers are thermodynamically unstable relative to more densely packed states. Over time, polymer chains relax toward a lower free-energy configuration, leading to shrinkage

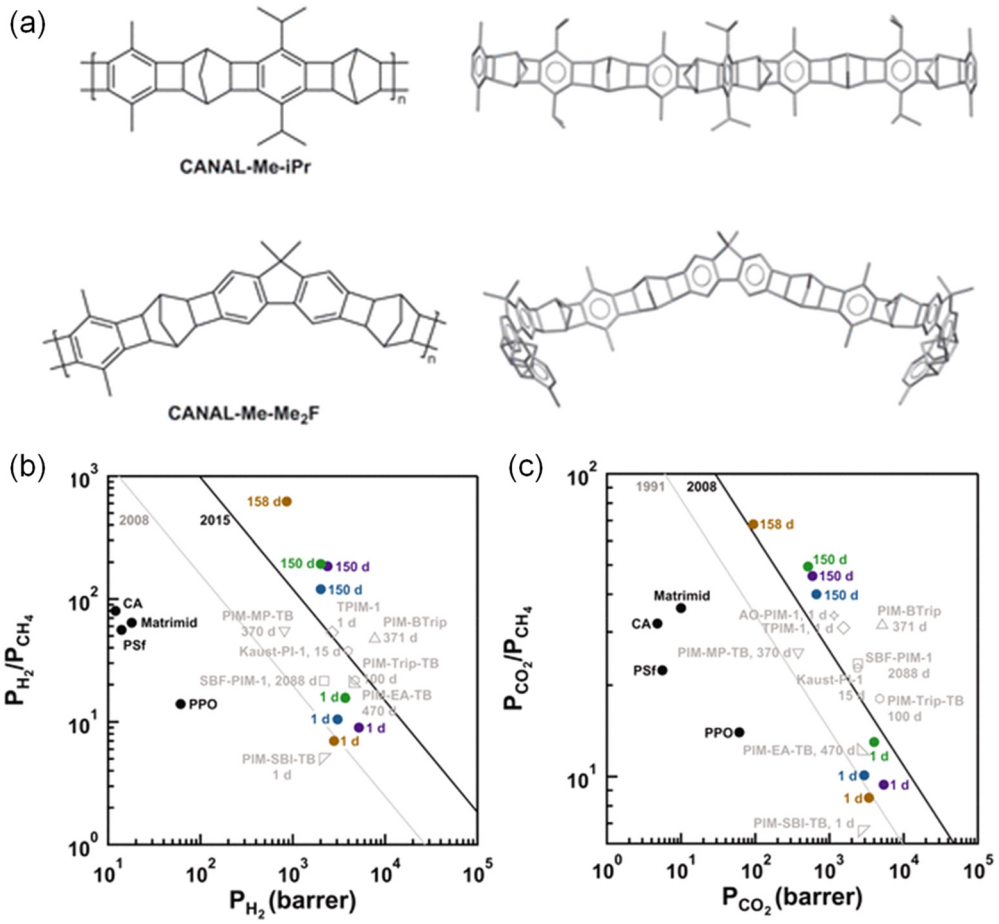

Fig. 13 (a) (Left) Experimental and (right) molecular-mechanics–simulated structures of a ribbonlike 2D ladder polymer (CANAL-Me-^{i}Pr, top) and a 3D ladder polymer (CANAL-Me-Me2F, bottom). Me = methyl; ^{i}Pr = isopropyl. (b) and (c) Pure-gas permeation data for 50–60 μm thick films of CANAL-Me-Me_2F (purple), CANAL-Me-S5F (green), CANAL-Me-S6F (blue), and CANAL-Me-DHP (brown), plotted relative to the (b) H_2/CH_4 and (c) CO_2/CH_4 upper bounds.[69] Reproduced from ref. 69 with permission from The American Association for the Advancement of Science, copyright 2022.

of micropores and corresponding reductions in permeability.[37] Aging rates are strongly thickness-dependent, with submicrometer films experiencing accelerated densification. PIM-1, for example, may lose more than half of its CO_2 permeability within weeks when cast as a 100-nm film.[70,71] This rapid aging poses serious limitations for industrial translation, where long-term stability is critical.

Several strategies have been developed to mitigate physical aging in PIMs.[37] Crosslinking—through thermal, chemical, or UV-assisted methods—can dramatically slow the relaxation of micropores, preserving permeability over extended timescales. Bridging functional groups can be introduced into the polymer backbone to reduce segmental mobility. Annealing treatments at controlled temperatures remove trapped solvent and stabilize free volume without erasing microporous architecture. Additionally, blending PIMs with more rigid polymers or incorporating inorganic fillers into mixed-matrix membranes (MMMs) can reinforce structural stability and reduce collapse of micropores. Among these strategies, ladderization and rigidification have proven particularly effective, reducing the magnitude of aging while retaining the permeability advantages characteristic of PIMs.[54,72–74]

CO_2 plasticization constitutes a second major challenge.[55] Due to their high affinity for CO_2 and flexible or semi-flexible linkages in some PIM architectures, penetrant-induced swelling can compromise size-sieving properties at elevated pressures. The propensity for plasticization underscores the delicate balance between diffusivity and mechanical stability inherent in ultrapermeable polymers. For high-pressure applications such as CO_2/CH_4 separation in natural gas processing or CO_2 removal in blue hydrogen production, strategies such as crosslinking, introducing bulky substituents, or incorporating rigid fused rings are necessary to suppress swelling and maintain selectivity.

Post-synthetic modification (PSM) has emerged as a highly practical strategy to tailor gas transport and stability in polymers of intrinsic microporosity (PIMs) without requiring entirely new polymer syntheses. The archetypal PIM-1, with its nitrile-functionalized backbone, provides a versatile reactive platform for introducing polar functionalities that modulate intermolecular interactions and pore structure. Through selective chemical transformations, the nitrile groups of PIM-1 can be converted into various derivatives containing carboxylic acid,[75] amine,[36] amidoxime,[76] tetrazole,[77] thioamide,[78] aldehyde,[79] or ketone[80] groups. These chemical modifications typically enhance gas selectivity and plasticization resistance by increasing interchain interactions, though often at the expense of reduced permeability due to matrix densification.

Among these modifications, amidoxime-functionalized PIM-1 (AO-PIM-1) has drawn particular attention for its potential in sour gas separation, where membranes must maintain CO_2 selectivity and stability under streams containing acidic contaminants such as H_2S.[76] The amidoxime group introduces both hydrogen-bonding capability and moderate basicity, improving CO_2 solubility while suppressing competitive sorption of non-polar gases. Furthermore, its chelating nature enhances chemical robustness against acid gases that typically degrade conventional PIMs. These materials demonstrate that appropriate PSM can extend the application of PIM-based membranes from idealized binary gas mixtures to complex industrial feeds while maintaining long-term performance.

Recent advances have expanded PSM beyond simple chemical functionalization toward controlled topological transformation of the polymer backbone. A representative breakthrough is the development of ladder-branched polyimides of intrinsic microporosity (PIM-PIs) *via* photoinduced [4+4] cycloaddition between anthracene moieties integrated into the polymer chain (Fig. 14).[81] Upon ultraviolet irradiation, these moieties form covalent dianthracene linkages, generating a rigid ladder-branched architecture that introduces additional microporosity while simultaneously stabilizing free-volume elements. This approach represents the first post-synthetic modification strategy capable of achieving high separation performance, long-term stability, and solution processability within a single polymer platform. The resulting membranes combine high CO_2 permeability ($\sim$350 Barrer) with CO_2/CH_4 selectivities exceeding 30 under mixed-gas conditions (50 : 50 CO_2/CH_4 feed and up to 31 bar), surpassing previously reported upper bounds for mixed-gas separations. Moreover, the ladder-branched topology effectively mitigates physical aging and CO_2-induced plasticization, maintaining permeability and selectivity even under elevated pressures and extended operation. This work demonstrates how controlled post-synthetic network formation can transform the inherent limitations of high-free-volume polymers into structural advantages, defining a new direction for the practical design of stable and processable PIM-based membranes.

In summary, PIMs constitute one of the most important and influential classes of next-generation CO_2 separation materials. Their inherent microporosity, tunable chemical structures, and extraordinary gas transport properties have reshaped the theoretical landscape of polymer membrane performance. At the same time, their vulnerabilities—rapid aging, plasticization, and thin-film brittleness—highlight the intricate interplay between molecular architecture and macroscopic membrane behavior. The evolution from first-generation PIM-1 to state-of-the-art CANAL polymers illustrates a clear trajectory toward advanced materials that preserve the permeability advantages of intrinsic microporosity while mitigating its drawbacks. These design principles and lessons directly inform the development of other polymer families, including the CO_2-philic ether-rich systems discussed in the next section, which approach permeability enhancement through a fundamentally different mechanism rooted in solubility selectivity rather than micropore-driven diffusivity.

3.3. Ether-rich CO_2-philic polymers (polyethers)

While TR polymers and PIMs derive their CO_2 separation performance primarily from diffusivity-driven mechanisms enabled by rigid, microporous architectures, a fundamentally different class of materials leverages thermodynamic affinity to achieve high CO_2 selectivity. Ether-rich polymers—most prominently polyethylene oxide (PEO)-based systems,[82] poly(1,3-dioxolane) (PDXLA),[83] and

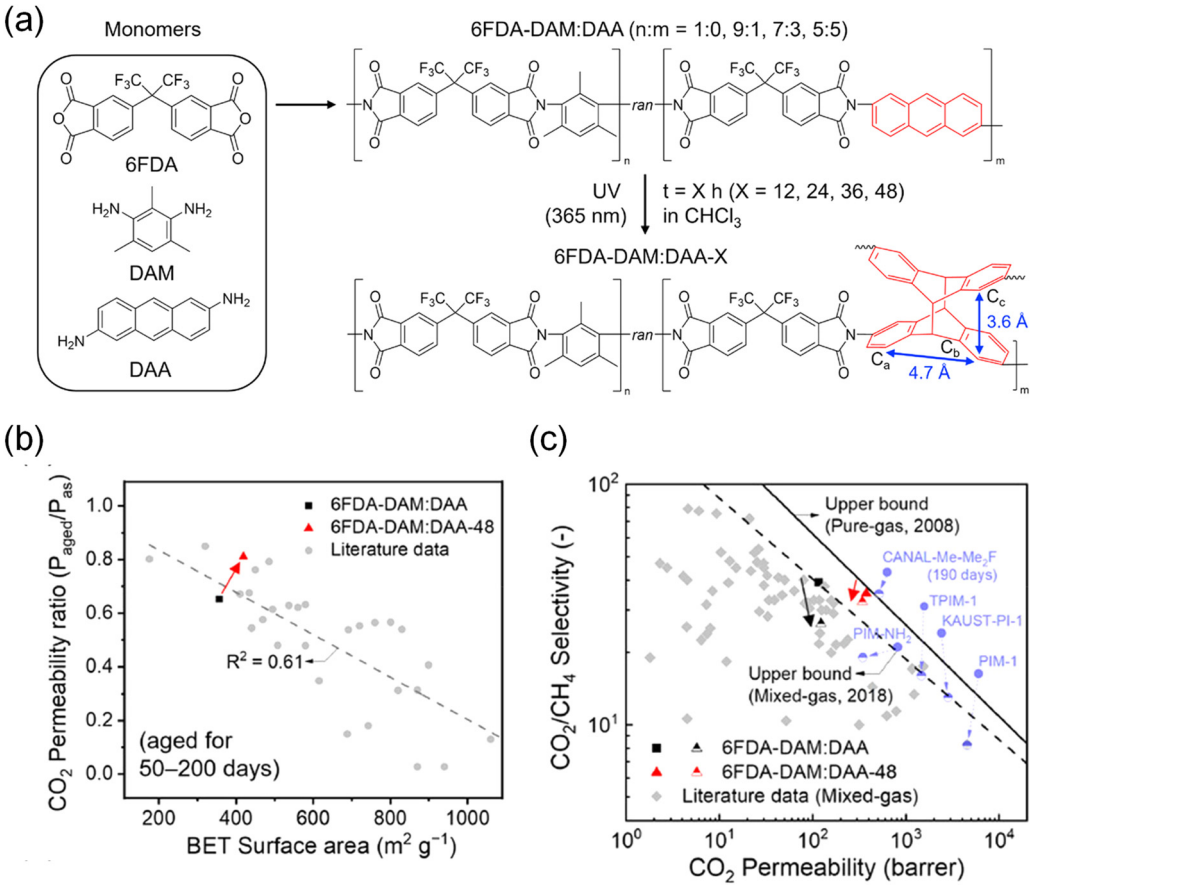

Fig. 14 (a) Synthesis of dianthracene-containing copolyimides (6FDA-DAM:DAA-X) *via* UV-induced [4+4] cycloaddition. Here, 6FDA is 4,4′-(hexafluoroisopropylidene) diphthalic anhydride, DAM is 2,4-diaminomesitylene, and DAA is 2,6-diaminoanthracene. Ran denotes that the materials are random copolymers. The illustrated distances between adjacent carbon pairs—two C_a carbons (4.7 Å) and two C_c carbons (3.6 Å)—are reproduced for clarity. (b) Plot of CO_2 permeability retention (P_{aged}/P_{as}) *versus* BET surface area (from N_2 sorption isotherms), shown alongside reported aging data (gray circles) for PIM-based membranes aged for 60–200 days. The dotted line represents a linear fit to the previously reported aging trend of PIMs. (c) CO_2/CH_4 mixed-gas separation performance of 6FDA-DAM:DAA and 6FDA-DAM:DAA-48 membrane films compared with literature data. Filled symbols represent pure-gas performance at 1 bar and 35 °C, whereas half-filled symbols represent mixed-gas performance at 31 bar and 35 °C using a 50 : 50 CO_2/CH_4 feed. The pure-gas and mixed-gas upper bounds are provided for ref. 81.

commercial block copolymers such as Pebax[84]—exemplify this solubility-selectivity-driven design philosophy. In these materials, strong dipole–quadrupole interactions between ether oxygens and CO_2 enhance solubility far beyond that of N_2 or CH_4, providing a powerful route toward selective CO_2 uptake even in the absence of extremely rigid backbones or intrinsic microporosity.[85,86] Early comparative studies revealed that introducing ether linkages significantly enhanced CO_2 sorption relative to hydrocarbon polymers like polyethylene, suggesting that polarity-driven solubility can be a powerful design lever for gas-selective membranes (Fig. 15).[85]

PEO represents the archetype of ether-rich CO_2-philic systems. The repeating –CH_2–CH_2–O– units provide dense populations of ether oxygens, leading to exceptionally high solubility selectivity for CO_2 over N_2 or CH_4. Indeed, early work demonstrated that CO_2 solubility in PEO could be up to an order of magnitude greater than in polyimides or polysulfones, making PEO one of the most CO_2-philic polymers known. However, this advantage is counterbalanced by significant barriers to practical membrane deployment. PEO has a relatively low glass transition temperature ($T_g \approx -60$ °C) and exhibits rubbery-chain mobility at ambient temperatures.[83,85,87] As a result, PEO-based materials suffer from low CO_2/CH_4 and CO_2/N_2 diffusivity selectivity and are often mechanically insufficient for producing thin, defect-free films.

Lin *et al.* first reported a systematic investigation of gas transport in PEO, providing fundamental insights into its separation behavior.[82] Pure PEO exhibited a CO_2 permeability of approximately 12 Barrer at 35 °C with a CO_2/N_2 selectivity of nearly 50, far exceeding that of polyethylene under identical conditions. The enhanced selectivity originates predominantly from CO_2 solubility rather than diffusivity, confirming the dominant role of ether–CO_2 interactions. However, the study also highlighted intrinsic limitations of PEO as a membrane material: its semicrystalline nature restricts segmental mobility and free volume in the amorphous phase, leading to relatively low overall gas permeability. Roughly 70% crystallinity was measured in typical PEO films, and transport was confined to

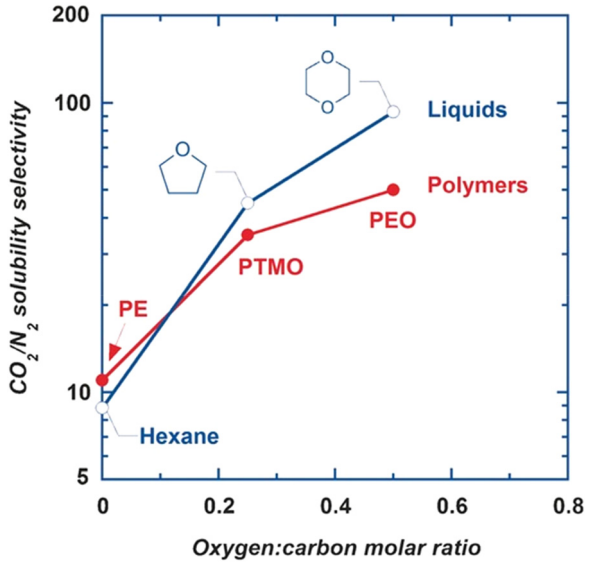

Fig. 15 Effect of increasing ether oxygen content in liquids and polymers on enhancing CO_2/N_2 solubility selectivity. PE = polyethylene; PTMO = poly(tetramethylene oxide); PEO = poly(ethylene oxide).[85] Reproduced from ref. 85 with permission from John Wiley and Sons, copyright 2016.

amorphous regions interspersed between impermeable crystalline domains. As a result, while PEO shows excellent CO_2/N_2 discrimination, its permeability remains modest compared to high-free-volume glassy polymers.

To address the inherent limitations of semicrystalline (PEO), researchers have pursued cross-linking of low–molecular-weight PEO oligomers (*i.e.*, polyethylene glycol, PEG), forming amorphous networks such as cross-linked poly(ethylene glycol) diacrylate (XLPEGDA) (Fig. 16).[88,89] The ether oxygens in these polymers provide strong interactions with CO_2, while the cross-linked architecture disrupts long-range crystallinity, maintaining flexible amorphous domains that facilitate gas transport. Early systematic studies demonstrated that when PEO segments between

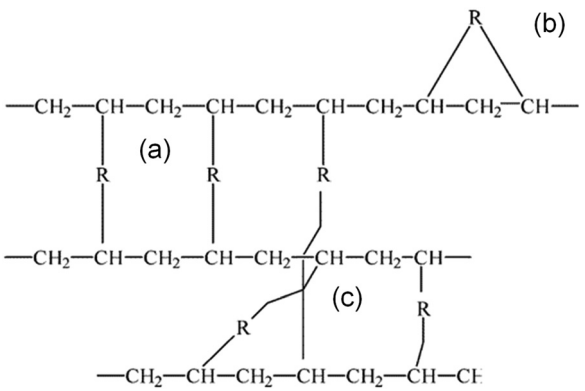

Fig. 16 Schematic representation of typical network elements in XLPEGDA. PEGDA features the repeating unit $CH_2CH–R–CHCH_2$. (a) The smallest possible network segment; (b) a wasted cross-link or loop; (c) an entanglement that becomes permanent due to cross-linking.[88] Reproduced from ref. 88 with permission from American Chemical Society, copyright 2005.

cross-links are shorter than about 1500 g mol^{-1}, the material remains fully amorphous and exhibits CO_2 permeability exceeding 500 Barrer—an order of magnitude greater than semicrystalline PEO—while preserving excellent CO_2/N_2 selectivity near 50.[88,89]

A later study introduced the concept of reverse selectivity in amorphous cross-linked PEO systems.[90] Under specific conditions of CO_2 plasticization, these materials exhibit CO_2/H_2 selectivity approaching 10, which is opposite to conventional molecular-sieving behavior where smaller gases permeate faster. This unusual trend arises because CO_2 diffusion is enhanced by transient swelling of the flexible amorphous matrix, while smaller, less condensable gases remain relatively unaffected. The work not only revealed the unique solubility-dominated transport in ether-rich polymers but also highlighted how controlled plasticization can be beneficial rather than detrimental to separation performance. However, despite their excellent gas transport properties and scientific significance, these cross-linked PEO-based materials are typically prepared as freestanding bulk films due to the limitations of photopolymerization methods. Their mechanical brittleness and lack of thin-film processability restrict their immediate applicability in practical gas-separation modules, rendering them more suitable for fundamental transport studies than for scalable membrane fabrication.[91] Nevertheless, the insights gained from XLPEGDA and related systems continue to guide the molecular design of amorphous, CO_2-philic polymers for next-generation membrane materials.[85]

To overcome these constraints, a new class of poly(1,3-dioxolane) (PDXLA)-based polymers was developed as amorphous, highly CO_2-philic alternatives with tunable chain architectures. The rationale was to increase ether oxygen content beyond that of PEO (O:C = 0.5) to improve CO_2 solubility selectivity, while avoiding the crystallization that typically plagues polar polymers. A molecularly engineered series of PDXLA copolymers was synthesized by incorporating poly(1,3-dioxolane) branches terminated with flexible ethoxy groups into a highly branched amorphous matrix. This design introduced high ether oxygen density for CO_2 affinity while maintaining low glass transition temperatures and high fractional free volume. The optimized copolymer achieved CO_2 permeability up to 1400 Barrer and CO_2/N_2 selectivity of 64 under simulated flue gas at 70 °C—performance well above the conventional permeability–selectivity upper bound (Fig. 17).[83] Moreover, the material demonstrated stable mixed-gas separation even in humid conditions, confirming the robustness of its solubility-selective mechanism. These results validated the design principle that short polar branches and flexible chain ends can simultaneously enhance gas diffusivity and solubility without inducing crystallization.

Despite their outstanding intrinsic separation performance, early PDXLA membranes were still prepared as cross-linked, freestanding films due to insolubility of the networked structure, limiting their applicability in thin-film composite (TFC) fabrication.[87,92] Recent advances addressed this challenge by synthesizing soluble, high–molecular-weight bottlebrush PDXLA (bPDXLA) using controlled radical polymerization. These uncross-linked polymers preserved the high ether oxygen content and CO_2

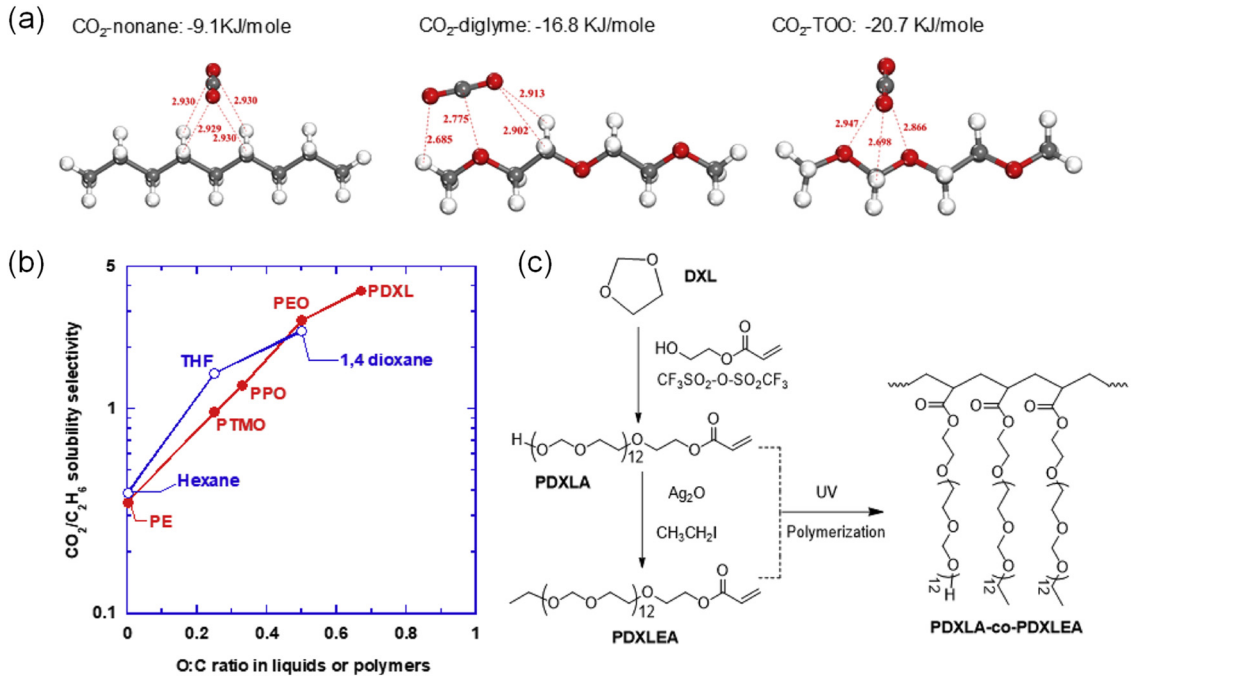

Fig. 17 (a) Simulated binding geometries of CO_2 with nonane, diglyme, and TOO. Bond lengths are shown in angstroms. Atom colors: C (gray), N (blue), O (red), H (white). (b) Influence of ether oxygen content in solvents (25 °C) and polymers (35 °C) on CO_2/C_2H_6 solubility selectivity. Representative polymers include polyethylene (PE), poly(tetramethylene oxide) (PTMO), and poly(propylene oxide) (PPO). (c) Schematic representation of the synthetic pathways for macromonomers (PDXLA and PDXLEA) and the preparation of highly branched polymers.[83] Reproduced from ref. 83 with permission from Elsevier, copyright 2019.

selectivity of PDXLA while enabling solution processing into nanofilm composite membranes *via* standard dip-coating. When blended with small amounts of poly(ethylene glycol) dimethyl ether (PEGDME) as a miscible plasticizer, the resulting nanofilms exhibited CO_2 permeance up to 1300 GPU with CO_2/N_2 selectivity around 50—matching or exceeding commercial membranes.[92]

Block copolymer architectures—such as hard-block–soft-block systems in which PEO serves as the CO_2-philic phase—lend structural integrity while maintaining solubility selectivity.[30,85,86] Pebax®, a widely studied poly(ether-*block*-amide), exemplifies this strategy: its polyamide hard segment provides mechanical strength and mitigates chain mobility, while its polyether soft segment confers high CO_2 affinity (Fig. 18).[84] Pebax membranes exhibit competitive CO_2 permeability, moderate selectivity, and excellent processability, making them ideal candidates for post-combustion CO_2 capture and the production of thin-film composite (TFC) architectures.

Early systematic studies demonstrated that CO_2/N_2 selectivity increased with the fraction of polar ether segments, reaching values as high as 56, while CO_2/H_2 selectivity approached 10—a rare example of "reverse selectivity" where CO_2 permeates faster than smaller hydrogen molecules.[84,93,94] These results established Pebax as one of the earliest commercially available polymer systems achieving high CO_2 solubility selectivity with robust mechanical integrity. Subsequent investigations explored the effects of block composition and soft-segment chemistry on gas transport. Increasing polyether content improved permeability, while more polar PEO segments favored CO_2 selectivity over less

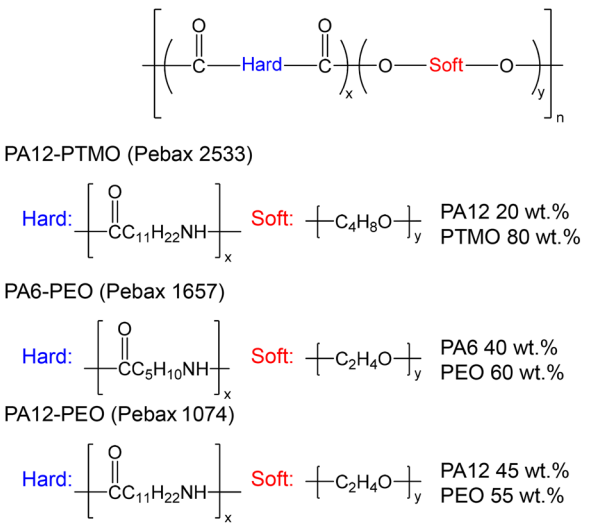

Fig. 18 Chemical structures of the Pebax polymers. PA6 = polyamide 6, PA12 = polyamide 12, PEO = poly(ethylene oxide), PTMO = poly(tetramethylene oxide).

polar PTMO analogues. Distinct Pebax grades, such as 1074, 1657, and 2533, exhibit tunable transport behavior depending on the balance between soft and hard segments. Blending Pebax with poly(ethylene glycol) methyl ether (PEGME) or ionic liquids further enhanced CO_2 solubility and reduced diffusion resistance, providing routes to tailor performance for specific separations such as post-combustion capture and natural gas sweetening.[30,95,96]

Recent studies have demonstrated that fine-tuning the nanoscale morphology of Pebax membranes is key to simultaneously improving gas permeability and selectivity. One investigation revealed that inducing controlled microphase reorganization within the block copolymer promotes more continuous PEO-rich transport channels while suppressing excessive crystallization (Fig. 19).[97] This optimized morphology enhanced the balance between CO_2 diffusivity and solubility, leading to a substantial improvement in separation performance without compromising selectivity. Another study focused on process-level optimization through interfacial and structural engineering of TFC membranes. By combining hydrophilic surface modification of the gutter layer with solvent vapor–induced rearrangement of the Pebax selective layer, the membrane exhibited a denser yet more permeable morphology with improved interlayer adhesion. These findings collectively underscore that coupling molecular-scale morphology control with interfacial engineering provides an effective route to enhance both the intrinsic and practical performance of Pebax-based membranes for scalable CO_2 capture applications.

Notably, PEO-based block copolymers also demonstrate attractive humidity tolerance. Unlike many glassy polymers in which water acts as a plasticizer or disrupts size-sieving pathways, ether-rich systems often benefit from water's presence. Water molecules can preferentially sorb into the ether-rich regions and enhance CO_2 solubility through plasticized microenvironments, which may increase permeability under flue gas conditions. This humidity-compatible behavior contrasts sharply with many glassy polymers and highlights the adaptability of PEO-containing materials to real industrial feeds.[98,99]

Ether-rich systems also excel in forming high-quality ultrathin selective layers in TFC membranes. Since ether-containing polymers generally exhibit good solubility in a wide range of solvents and possess moderate viscosity in coating solutions, they lend themselves readily to dip-coating, spin-coating, and bar-coating processes. Pebax, for example, routinely forms ~100–300 nm defect-free selective layers with excellent adhesion to gutter layers and porous supports.[30,31] Their mechanical flexibility mitigates the brittleness encountered in PIM- or TR-based thin films, significantly reducing the risk of pinhole formation. This coating ease contributes to their favorable techno-economic prospects for large-scale CO_2 capture applications. The broad processability of ether-rich polymers enables their integration with advanced membrane device architectures, including hollow fibers. However, their performance in high-pressure applications remains limited by swelling and plasticization, yielding relatively low CO_2/CH_4 selectivity. Consequently, they are more compelling as candidate materials for post-combustion and low-pressure CO_2 capture rather than for natural gas sweetening.

Overall, ether-rich CO_2-philic polymers offer a compelling complement to diffusivity-selective high-free-volume materials. Their solubility-driven selectivity mechanism is fundamentally different from the micropore-based transport strategies of TR polymers or PIMs, allowing them to excel in environments where humidity is high, operating pressures are moderate, and coating processability is a priority. Although their susceptibility to swelling and plasticization limits their applicability in high-pressure separations, their processability, thin-film compatibility, and strong CO_2 affinity make them ideal candidates for post-combustion capture, biogas purification, and integration into advanced TFC architectures.

In combination with the diffusivity-focused polymer classes described earlier, ether-rich polymers complete a threefold landscape of design philosophies for polymeric CO_2 separation membranes: rigid microporous backbones (TR), contorted

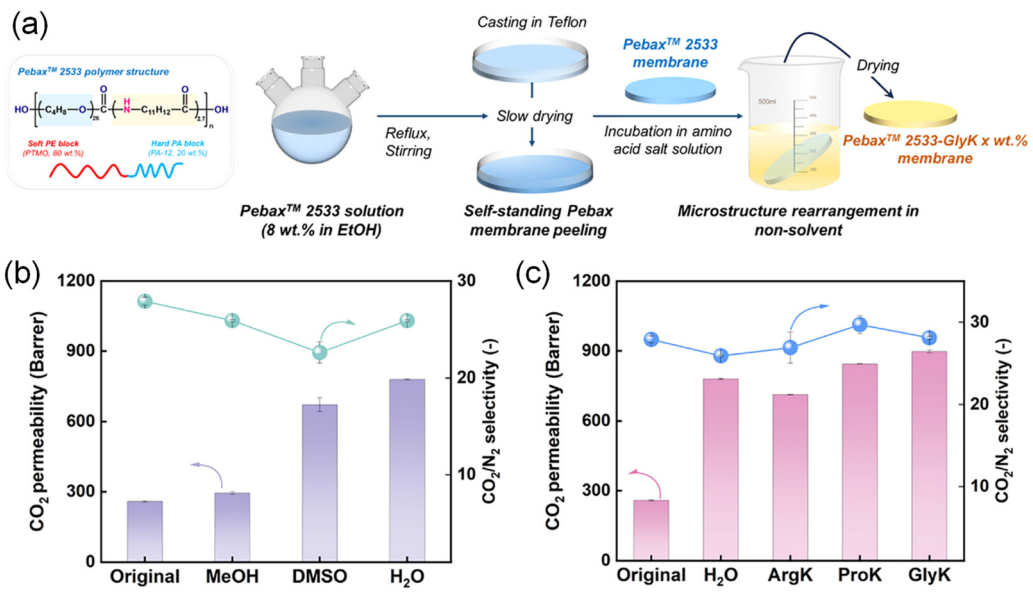

Fig. 19 (a) Schematic illustration of the non-solvent–induced microstructure rearrangement (MSR) fabrication procedure. (b) Comparison of gas transport properties for membranes treated with DI water and various organic solvents. (c) Gas permeation characteristics of membranes exposed to 2 wt% aqueous amino acid salt solutions. All measurements were conducted at 25 °C under a feed pressure of 2 bar.[97]

ladder architectures (PIMs), and solubility-selective flexible systems (ether-rich polymers). Each family provides distinct advantages and limitations, underscoring the importance of matching polymer chemistry to process conditions and module architecture. The diverse mechanisms governing transport, stability, and morphology across these materials demonstrate that no single polymer is universally optimal for all CO_2 separation scenarios. Rather, the future of membrane-based CO_2 capture will depend on rational integration of material design with process requirements, as explored in the following section on markets and technological opportunities.

4. Beyond dense films: importance of thin-film engineering

4.1. Knowledge gap between permeability and permeance

Over the past few decades, extensive studies on dense polymer films have established the foundation for understanding gas transport and have driven the evolution of polymeric membranes for CO_2 separation. Indeed, the accumulation of intrinsic permeability data enabled the formulation and continual refinement of the empirical upper bounds introduced in 1991 and later redefined in 2008 and 2019, reflecting the rapid progress in high-free-volume polymers such as PIMs and advanced polyimides. However, the transition from thick, free-standing dense films to practical thin TFC or ISA membranes revealed a major disparity between intrinsic permeability and the actual permeance achieved in real devices.

As highlighted in recent analyses, this ''knowledge gap'' originates from structural and interfacial limitations that arise when a polymer is processed into an ultrathin layer (<1 μm). The selective layer's morphology, interfacial defects, and the intrinsic resistance of porous supports or gutter layers often distort the ideal diffusion behavior predicted from bulk properties. For example, Fujikawa *et al.* demonstrated that interfacial nanoblending between Pebax and poly(dimethylsiloxane) (PDMS) layers can significantly alter CO_2/N_2 selectivity, contradicting the simple resistance-in-series model (Fig. 20).[100] This finding underscores that molecular-level interactions at the interface—rather than the intrinsic permeability of the bulk material—can dominate the overall performance of TFC membranes.

As Wu *et al.* noted,[19] many laboratory-scale polymers with outstanding CO_2/N_2 permeability–selectivity combinations fail to maintain comparable performance after being fabricated into practical TFC configurations. The challenge is not solely in discovering new materials but in translating intrinsic permeability into scalable membrane permeance through rational thin-film engineering. Therefore, bridging the gap between permeability and permeance requires integrating molecular design with interfacial control, support optimization, and accurate resistance modeling. Understanding how ultrathin selective layers interact with underlying substrates and how interfacial morphology governs gas transport is essential for transforming record-setting dense-film materials into viable modules for industrial CO_2 capture.

Motivated by these studies, we compared CO_2 separation performance plotted using permeability measured from dense films with that plotted using permeance measured from thin selective layers represented by TFC membranes. To highlight the impact of membrane thickness on performance, post-combustion CO_2 capture (*i.e.*, CO_2/N_2 separation) is adopted as a representative case, since higher permeance is well known to translate directly into substantial reductions in CO_2 capture cost.[13]

For dense films, the development of TR polymers, PIMs, and polyether-based polymers has indeed led to superior CO_2/N_2 separation performances that far exceed those of conventional commercial polymers such as Matrimid®, CA, and PSf, thereby defining the 2008[14] and 2019[15] upper bounds (Fig. 21a). When these materials are ideally assumed to be coated as 0.1 μm-thick selective layers, several tens of candidates already fall within the target performance window for post-combustion CO_2 capture.

In contrast, the reported data of TFC membranes reveal several notable trends (Fig. 21b). First, the clearly localized performance clusters observed for different material classes in

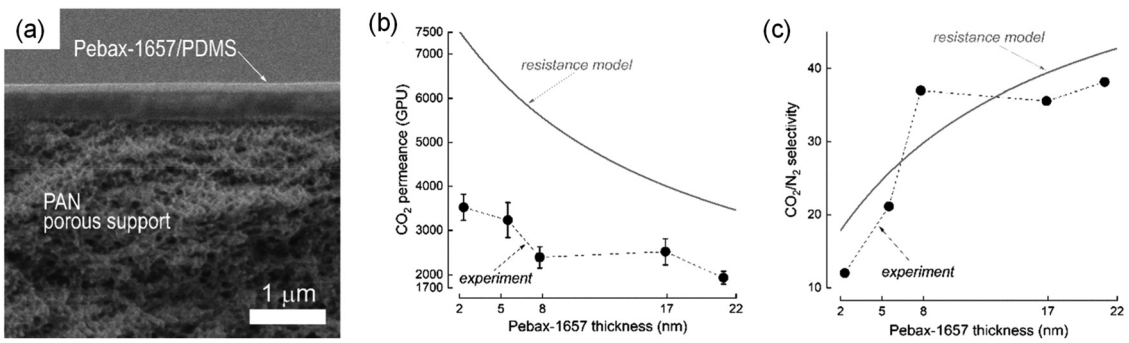

Fig. 20 (a) Cross-sectional images of the TFC membrane featuring an approximately 10 nm–thick Pebax-1657 selective layer. (b) and (c) Influence of selective-layer thickness on gas transport. Experimental results for (b) CO_2 permeance and (c) CO_2/N_2 selectivity of PDMS5/O20.7/Pebax TFC membranes are compared with predictions from the resistance-in-series model.[100] Reproduced from ref. 100 with permission from American Chemical Society, copyright 2020.

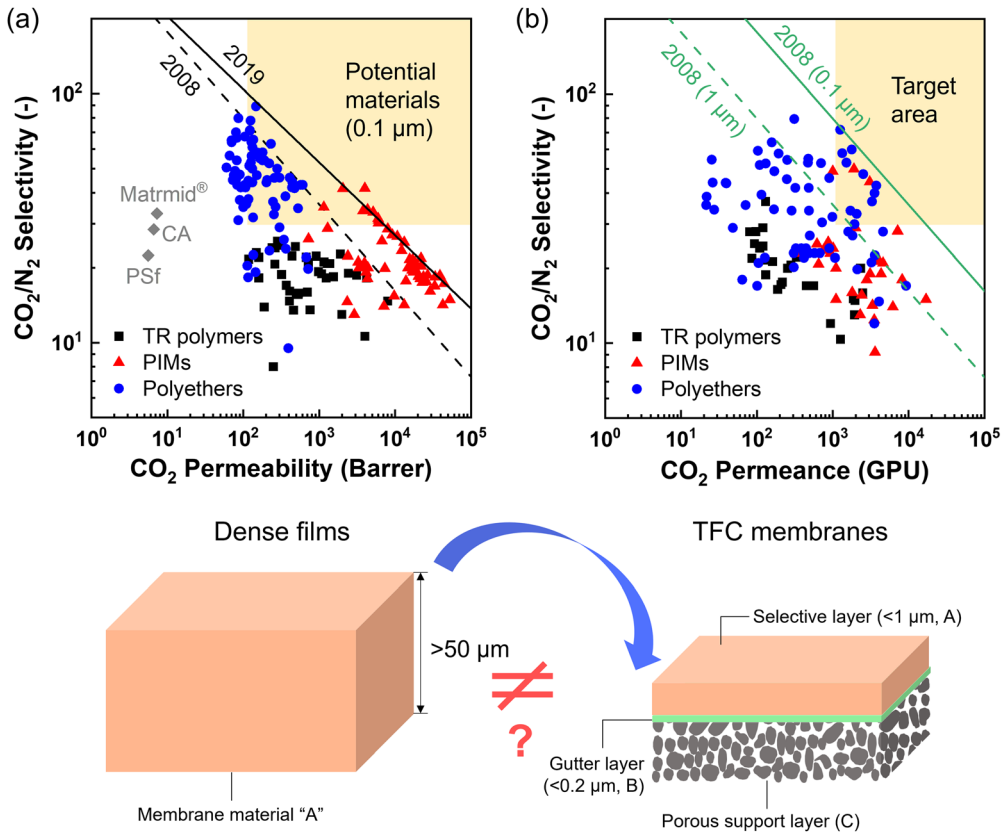

Fig. 21 Proposed knowledge gap between intrinsic material performance (*i.e.*, permeability) and practical membrane performance (*i.e.*, permeance). (a) Literature survey of CO_2 permeability (unit: Barrer) measured from dense films of TR polymers, PIMs, and polyether-based polymers.[14,15,23,38,81] The black dashed and solid lines represent the 2008[14] and 2019[15] upper bounds for polymeric membranes for CO_2/N_2 separation, respectively. The yellow box indicates candidate materials that could reach the target performance for post-combustion capture when coated as a 0.1 μm-thick selective layer.[13] (b) Literature survey of gas permeance (unit: GPU) measured from TFC membranes.[23,38,101] The green dashed line denotes the separation performance upper bound for a 1 μm-thick selective layer derived from the 2008 upper bound,[14] while the green solid line denotes the corresponding upper bound for a 0.1 μm-thick selective layer. The yellow box indicates the target CO_2/N_2 separation performance for post-combustion capture.[13] Most separation performances were measured at temperatures ranging from 25 to 35 °C and pressures from 1 to 2 bar, including both pure-gas and mixed-gas CO_2/N_2 separation data. Of note, facilitated transport membranes are also important candidates for CO_2 separation; however, they are excluded here because standardized benchmarks for a fair comparison with solution-diffusion-mechanism-based polymer membranes are not yet established. All data presented herein are sourced from ref. 101.

dense films become highly mixed. Second, the performance distribution within the same material class is significantly more scattered. Third, unlike the dense-film-based projection, only a limited number of TFC membranes reach the target separation performance region. Fourth, and most strikingly, despite the apparent potential to access the target region when a 0.1 μm-thick ultrathin layer is assumed based on the 2008 upper bound,[14] no reported TFC membrane surpasses the corresponding 0.1 μm-based upper bound.

These observations indicate that intrinsic material performance inferred from permeability does not translate directly into practical membrane performance expressed in terms of permeance. In other words, a clear knowledge gap exists between dense-film properties and thin-film membrane behavior. Although this comparison is idealized and does not explicitly account for resistance of the support layer, interfacial effects, or the intensified plasticization, physical aging, and structural changes that become more pronounced in ultrathin films, which will be discussed in the following sections, the results nevertheless highlight a critical imbalance: thin-film engineering has lagged behind material development, and this disparity is a key contributor to the observed knowledge gap. In the following sections, these critical phenomena associated with the bulk-to-thin-film transition will be discussed in detail to elucidate their collective impact on the performance and stability of practical CO_2 separation membranes.

4.2. Intensified plasticization in thin films

Early studies by Paul *et al.* established that polymer thin films exhibit significantly stronger and faster CO_2-induced plasticization than their bulk counterparts.[70,71,102] Using polyimide membranes as a model system, they demonstrated that as film thickness decreases from micrometers to hundreds of nanometers, the onset of plasticization shifts to lower pressures and the permeability rises more sharply with CO_2 exposure (Fig. 22).

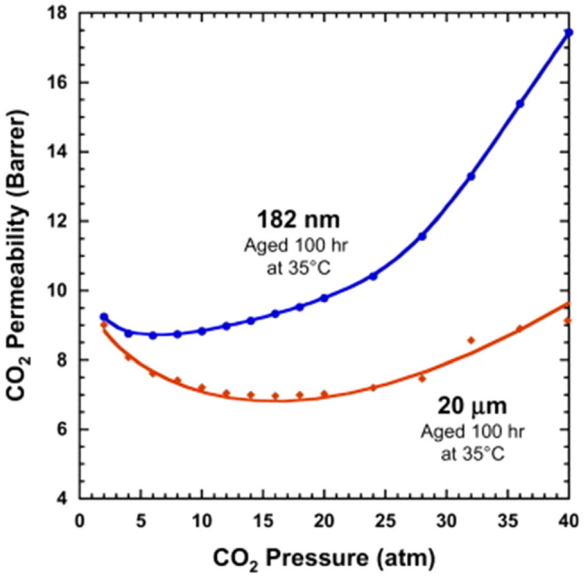

Fig. 22 CO_2 plasticization pressure profiles for thin (182 nm) and thick (20 μm) Matrimid® films prepared with identical thermal histories.[70] Reproduced from ref. 70 with permission from Elsevier, copyright 2011.

This enhancement originates from the greater chain mobility and shorter relaxation times in confined films, where free-volume elements can reorganize more readily under penetrant sorption. Their follow-up investigations revealed that thin films not only plasticize more rapidly but also experience conditioning effects—irreversible microstructural rearrangements that persist after CO_2 removal—further distinguishing nanoscale transport from bulk behavior.[71]

Building on this foundation, Pinnau *et al.* systematically examined CO_2 sorption and dilation phenomena in ultrathin PIM-1 using *in situ* ellipsometry.[103,104] They found that reducing film thickness below 100 nm markedly amplifies swelling, reaching nearly threefold greater volumetric expansion at 7 nm compared to 128 nm films. This pronounced plasticization was attributed to the highly nonequilibrium, loosely packed nature of ultrathin PIM layers, which relax mechanical stress through enhanced swelling under high-pressure CO_2. Their analysis also showed that nanoconfinement lowers the apparent glass transition temperature by over 200 °C relative to bulk, indicating a transition toward more rubbery-like behavior.

Recent mixed-gas and TFC-based studies extended these observations to practical membrane configurations. Acid-hydrolyzed PIM-1 thin-film composites exhibited unusually high initial CO_2 permeabilities but suffered from selectivity loss under CO_2-rich feeds, confirming that plasticization remains more severe in sub-micrometer selective layers than in thick films.[105] Collectively, these results reveal that the reduction of membrane thickness intensifies CO_2-induced chain relaxation and free-volume expansion—transforming plasticization from a manageable bulk effect into a dominant instability mechanism that must be explicitly addressed in thin-film membrane design.

4.3. Accelerated physical aging in thin films

The phenomenon of accelerated physical aging in thin polymer films has been extensively investigated to understand how confinement alters structural relaxation and gas transport properties. Early experimental studies using PALS revealed that, unlike bulk samples, submicrometer PIM-1 films lose free volume rapidly—often completing the majority of aging within a few months.[106] The decay of positronium lifetime and intensity across film depth demonstrated that free volume diffuses toward the surface rather than collapsing uniformly throughout the matrix. This observation provided the first mechanistic evidence that nanoconfinement facilitates out-diffusion of excess free volume, leading to faster densification and permeability loss than in bulk materials.

Subsequent systematic work by Tiwari *et al.* established the quantitative relationship between thickness and aging rate in PIM-1 membranes.[71] Comparing thick (tens of micrometers) and thin (hundreds of nanometers) films, they found that permeability decay after 1000 hours was 67% for thin films *versus* 53% for thick ones, confirming that structural relaxation accelerates as the active layer becomes thinner. The authors also noted that film processing history—including casting solvent and methanol treatment—strongly influences the initial free volume and hence the aging trajectory. Methanol-soaked films, while initially more open, exhibited rapid densification due to solvent-induced chain rearrangement. Furthermore, exposure to CO_2 revealed that thin films experience competing plasticization and aging effects, with aging dominating within minutes of gas sorption, suggesting that nanoscale confinement amplifies both dynamic and thermodynamic relaxation phenomena.

Later investigations expanded this understanding by examining structural and topological effects. Highly aged TFC membranes, as reported by Lee *et al.*, further revealed that excessive relaxation in thin selective layer can lead to irreversible densification and performance decline—referred to as "hyper-aging".[107] They observed that even moderate thermal or pressure exposure accelerated free-volume collapse at rates far exceeding those predicted from bulk kinetics, emphasizing that interfacial stresses and nanoconfinement jointly dictate long-term stability (Fig. 23). Interestingly, Budd *et al.* showed that the aging-induced densification of PIM-1 is not entirely irreversible.[108] They demonstrated that short methanol vapor exposure can rejuvenate aged thin-film composites by reopening collapsed micropores and restoring permeability nearly to the pristine level (Fig. 24). This reversible plasticization–relaxation interplay provides a new insight into the dynamic nature of free-volume evolution under confinement.

Overall, these findings indicate that thin-film confinement intensifies the physical aging of high-free-volume polymers through accelerated free-volume diffusion, enhanced surface mobility, and interfacial stress. Yet, the discovery of rejuvenation pathways also suggests that controlled vapor or solvent treatment could counteract densification, offering practical strategies to stabilize or even recover performance in next-generation thin-film composite membranes for CO_2 separation.

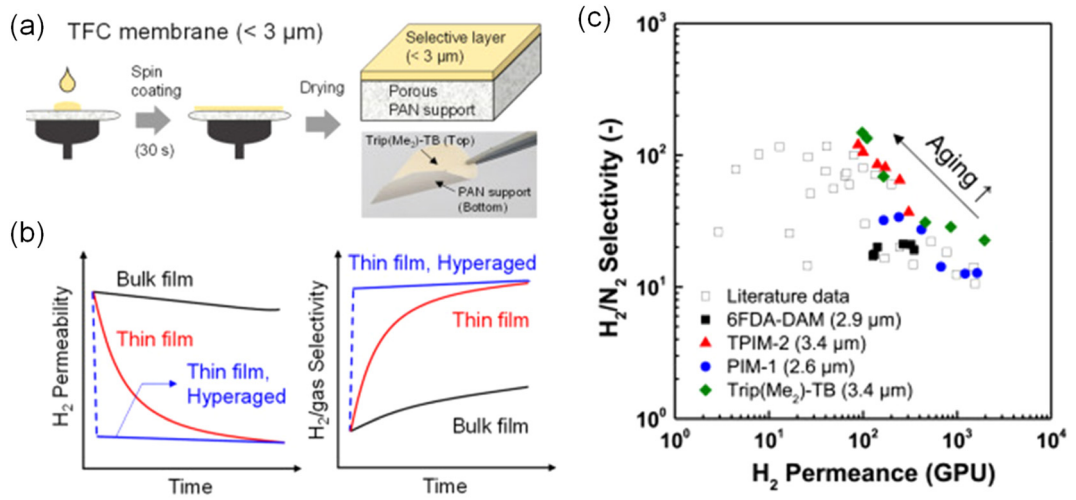

Fig. 23 (a) Schematic representation of the fabrication process for PIM-based thin-film composite (TFC) membranes. (b) Illustration of how physical aging influences H_2 separation in PIMs, comparing bulk films, thin films, and hyperaged thin films. (c) Comparison of H_2/N_2 separation performance for PIM-based TFC membranes with values reported in the literature. Arrows indicate the evolution of gas-separation properties over 0–336 h.[107] Reproduced from ref. 107 with permission from Elsevier, copyright 2023.

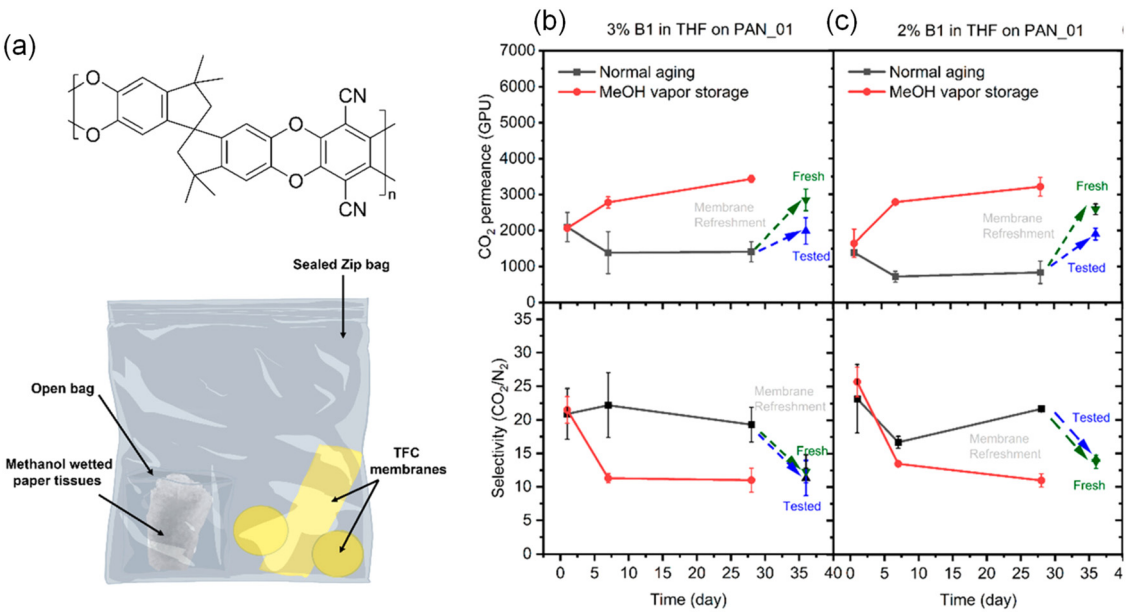

Fig. 24 (a) Chemical structure of PIM-1 and schematic of the methanol-vapor storage method used for PIM-1 TFC membranes. (b) and (c) Evolution of CO_2 permeance and CO_2/N_2 selectivity during aging of PIM-1 TFC membranes stored under ambient conditions *versus* methanol-vapor conditions. The TFC membranes were fabricated using branched PIM-1 from (b) 3% and (c) 2% THF solutions on PAN supports. Membranes previously subjected to gas permeation tests and subsequently retested are indicated as tested (blue), whereas membranes evaluated for the first time are indicated as fresh (green).[108]

4.4. Unexpected structural transitions in thin films

Thin-film polymer membranes exhibit complex structural transitions that are distinct from their bulk counterparts, often leading to unexpected transport behaviors.[19,109–112] Early studies on semicrystalline polymers such as PEO revealed that nanoscale confinement dramatically alters the crystalline phase. In ultrathin films, PEO transitions from its conventional spherulitic morphology to a highly oriented lamellar structure aligned parallel to the substrate, driven by interfacial energy minimization. This orientation reduces amorphous interlamellar regions and restricts chain mobility, which in turn suppresses gas diffusivity despite an overall increase in crystallinity (Fig. 25).[113] These findings established one of the first examples of how nanoscale film confinement can invert the conventional relationship between crystallinity and permeability.

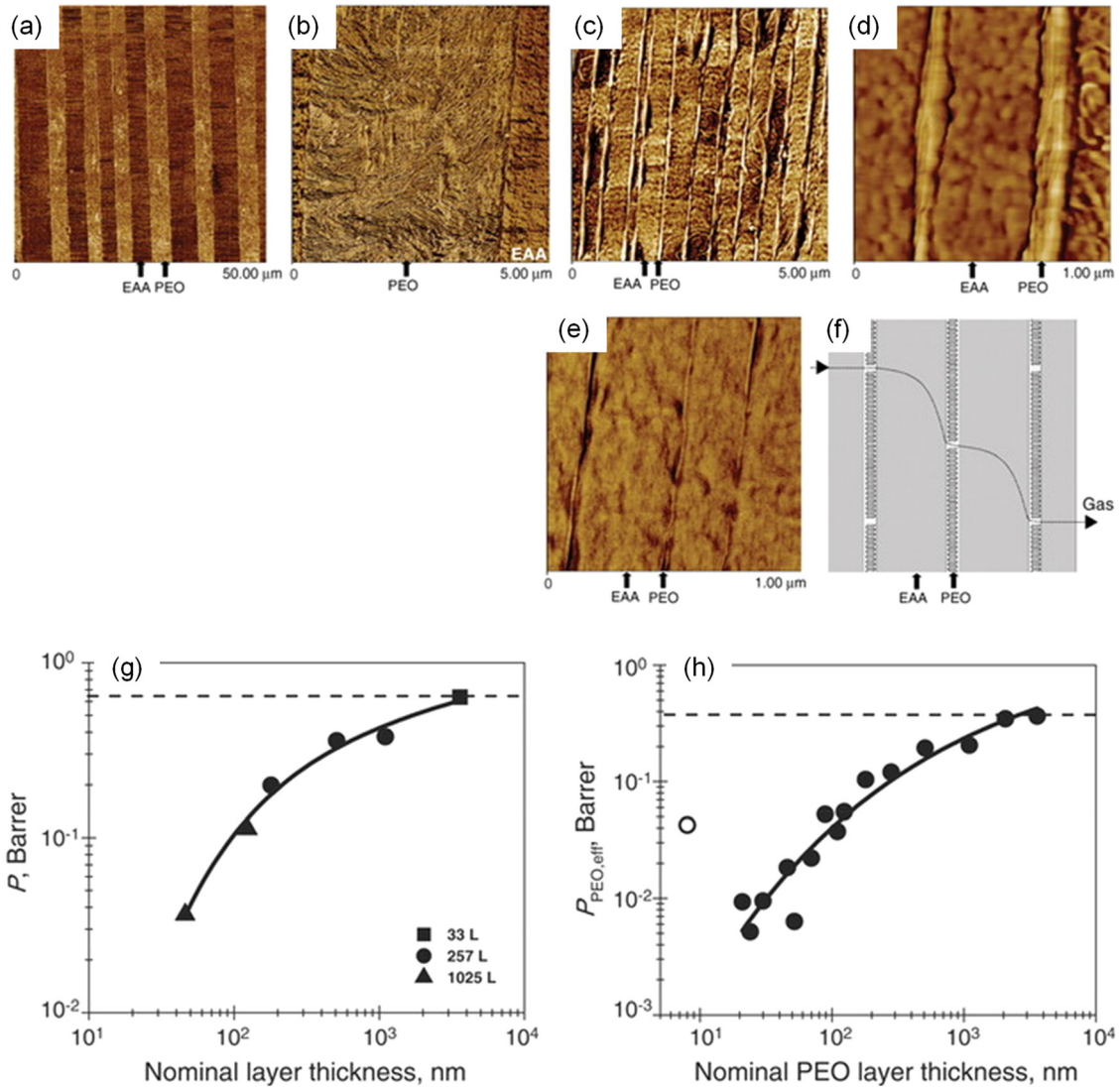

Fig. 25 (a)–(e) AFM phase images of partial cross sections of multilayer EAA/PEO films. Since the PEO layers exhibit much higher crystallinity than EAA, they appear bright in the images. (a) Low-resolution image of a 50/50 EAA/PEO film with 33 layers and a nominal PEO thickness of 3.6 μm. (b) High-resolution image highlighting the spherulitic morphology of the 3.6-μm PEO layer. (c) Low-resolution image of a 70/30 film with 1025 layers and 110-nm PEO layers. (d) High-resolution view showing oriented lamellar stacks within the 110-nm PEO layers. (e) High-resolution image of a 90/10 film with 1025 layers and 20-nm PEO layers, in which PEO crystallizes into single, very large lamellae. (f) Schematic of the gas-diffusion pathway through the layered assembly containing 20-nm PEO layers; arrows indicate EAA and PEO layers. (g) O_2 permeability of films containing equal volume fractions of EAA and PEO. (h) O_2 permeability of PEO layers across films of varying composition. The dashed line marks the permeability of pure PEO; the open symbol denotes a sample showing PEO layer breakup. Solid lines are guides to the eye.[113] Reproduced from ref. 113 with permission from The American Association for the Advancement of Science.

Similar structural reorganization has been observed in elastomeric and amorphous systems. For instance, investigations of PDMS films across a wide thickness range demonstrated that thinning below a few micrometers induces aggregation of polymer chains into low-dimensional fractal domains.[110] Small-angle scattering and calorimetry revealed an increase in crystalline ordering and a higher melting transition for ultrathin PDMS layers, while surface wetting experiments confirmed a concurrent loss of hydrophobicity. These effects were attributed to the increased prevalence of interfacial chain alignment and heterogeneous crosslinking density, producing a loose yet partially ordered network that enhances flux but compromises selectivity. Similarly, in CA membranes, X-ray diffraction and thermal analyses showed that solvent–substrate interactions during thin-film casting promoted localized densification and orientation of polymer backbones, yielding lower gas permeability than expected from bulk films despite the same chemical composition.[112,114]

More recent work on high-free-volume glassy polymers has revealed even more pronounced structural transitions. When polymers of intrinsic microporosity (PIMs) are fabricated into submicrometer films, the microstructure becomes strongly

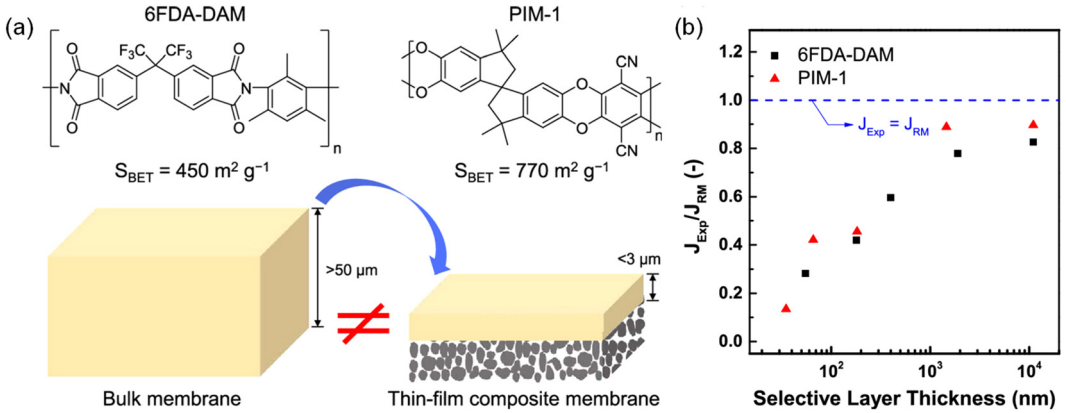

Fig. 26 (a) Conceptual schematic illustrating how structural and physical differences between PIM-based bulk membranes and thin-film composite (TFC) membranes lead to variations in CO_2 separation performance. (b) CO_2 Permeance ratio of experimental data (J_{Exp}) to resistance-model predictions (J_{RM}) for 6FDA-DAM and PIM-1 TFC membranes with varying selective-layer thicknesses.[115] Reproduced from ref. 115 with permission from American Chemical Society, copyright 2024.

anisotropic, as demonstrated by two-dimensional grazing-incidence X-ray scattering (GIXS). The isotropic micropore distribution of bulk films collapses into directionally aligned ultramicropores confined within the plane of the film, while out-of-plane micropores become disconnected (Fig. 26).[115] This anisotropy arises from rapid solvent evaporation and shear stresses during spin-coating, combined with confinement-induced restriction of interchain packing. As a result, PIM thin films exhibit lower permeance than predicted by bulk permeability data, and the deviation intensifies with decreasing thickness.

Overall, these studies reveal that structural transitions in thin polymer films—ranging from crystallization and aggregation in flexible polymers to anisotropic micropore evolution in glassy systems—are not merely secondary effects but central determinants of membrane performance. Understanding and controlling such confinement-induced phenomena are therefore critical to accurately translating bulk polymer properties into the high-permeance, stable thin-film membranes required for scalable CO_2 separation applications.

5. Markets and business outlook for polymeric CO_2 separation membranes

The global market landscape for gas separation membranes is undergoing rapid and structural transformation driven by decarbonization policies, expansion of hydrogen value chains, tightening environmental regulations, and increasing deployment of modular CO_2 capture technologies.[1–4] Historically dominated by natural gas sweetening and nitrogen generation, the membrane industry is now transitioning toward a broader set of opportunities that include post-combustion CO_2 capture, biogas upgrading, blue hydrogen production, and specialty separations. These emerging markets place new demands on membrane materials—higher permeance, improved stability, resistance to plasticization, and compatibility with humid or contaminated feeds—making the advances discussed in the previous sections directly relevant to industrial adoption.

The membrane industry is unique in that it sits at the intersection of materials innovation and process engineering.[9] While breakthroughs in polymer chemistry can shift the Robeson upper bound and unlock new performance regimes, commercial viability depends equally on the ability to fabricate reliable modules, integrate membranes into complex process flows, and deliver competitive techno-economics relative to incumbent technologies such as amine absorption, pressure swing adsorption (PSA), and cryogenic distillation. These factors define the practical constraints under which polymeric CO_2-separation membranes must operate and shape the direction of research and development (R&D) investments in both industry and academia.

5.1. Current market structure and growth drivers

The present-day gas separation membrane market—estimated at roughly USD 1–2.7 billion depending on the scope of technologies included—is dominated by polymeric hollow-fiber and spiral-wound modules deployed primarily for CO_2/CH_4 separation in natural gas processing and for N_2 generation from air.[8,10,11] Polyimide and CA membranes account for the majority of installed capacity, reflecting decades of validated performance, reliable module fabrication, and well-developed supply chains.

However, several macro-level changes are reshaping market dynamics. First, national decarbonization strategies, including carbon pricing, clean hydrogen mandates, and emissions standards in power and industrial sectors, are accelerating demand for CO_2-removal technologies. Second, the build-out of hydrogen hubs and blue hydrogen infrastructure requires high-performance membranes capable of purifying H_2 streams and removing CO_2 at high pressures.[1,116] Third, rapid growth in biogas upgrading—particularly in Europe, North America, and parts of Asia—has created a distributed market for modular CO_2/CH_4 separation systems that favor membranes for their operational simplicity and compactness.

In addition, sustained growth in petrochemical production, especially in Asia–Pacific regions, is increasing demand for membranes used in refinery off-gas treatment, olefin purification, and nitrogen removal. These combined drivers suggest mid-to-high single-digit annual growth rates for the membrane industry over the next decade, with CO_2 and H_2 separations expected to outpace broader market averages.

5.2. Application segments and required membrane characteristics

Natural gas sweetening (CO_2/CH_4). This remains the largest historical market for gas separation membranes. Feed compositions vary widely, with CO_2 concentrations ranging from a few percent to over 70% in sour gas fields. Membranes must operate at high pressures (20–60 bar) and exhibit strong CO_2/CH_4 selectivity while resisting severe plasticization.

Commercial polyimides have proven their reliability here, but the growing complexity of gas feeds and expansion to harsher operating conditions create demand for more stable materials. TR polymers and PIMs exhibit promising high-pressure stability and selectivity, but challenges in thin-film translation and plasticization control remain. Ether-rich systems, by contrast, are unsuitable due to excessive swelling at high CO_2 pressures.

Post-combustion CO_2 capture (CO_2/N_2). Post-combustion capture represents one of the largest potential markets for membranes but also one of the most demanding. Flue gas is near atmospheric pressure, contains 10–15% CO_2, and is highly humid, often with contaminants such as SO_x and NO_x. High CO_2 permeance (>1000 GPU) is essential to minimize membrane area and capital cost. Robustness to humidity and contaminants is equally critical.

Materials such as Pebax, PDXLA, and other ether-rich polymers show strong humidity tolerance and good CO_2 permeability. PIMs and TR polymers can offer exceptional intrinsic performance, but thin-film aging and defect formation remain major barriers. Composite architectures using highly permeable gutter layers and defect-healing coatings show promise for enabling ultrathin selective layers (<200 nm) based on high-free-volume polymers.

Blue hydrogen production (H_2/CO_2 separations). Hydrogen production *via* steam methane reforming (SMR) or autothermal reforming (ATR) generates a high-pressure mixture of H_2, CO_2, and small amounts of CH_4 and CO. Membranes can be deployed either upstream of PSA units to reduce CO_2 load or downstream for tail-gas upgrading.

High-pressure CO_2 removal requires materials with excellent plasticization resistance, favoring TR polymers and rigid ladder PIMs. Hydrogen purification demands extremely high H_2 permeance and selectivity, but polymeric membranes currently struggle to compete with PSA at high purity requirements. Nevertheless, membrane–PSA hybrids reduce energy consumption and capital cost, creating a growing business niche for high-stability polymeric modules.

Biogas upgrading (CO_2/CH_4). Biogas upgrading is expanding rapidly due to renewable fuel mandates and the growth of distributed waste-to-energy systems. Membranes are favored in this sector because systems operate at moderate pressures, require minimal operator intervention, and can be deployed at small scales.

Ether-rich systems such as Pebax exhibit favorable performance under humid biogas conditions, while TR and PIM membranes offer higher selectivity and permeance when stability challenges are addressed. Techno-economically, membranes have become the dominant biogas upgrading technology in several European markets.

5.3. Module and system-level considerations

While materials innovation drives intrinsic performance, module design determines real-world feasibility. Hollow-fiber modules dominate the commercial landscape because of their high packing density, mechanical robustness, and scalability. Polyimide-based hollow fibers have been optimized extensively, providing predictable performance and long operational lifetimes. However, translating advanced materials such as TR polymers, PIMs, and CANAL structures into hollow-fiber form remains one of the largest bottlenecks in next-generation membrane deployment. Brittleness, coating uniformity, adhesion, and stress concentration all present barriers to producing defect-free fibers. Most research efforts therefore focus on TFC flat-sheet modules, which are easier to fabricate but less scalable. Transport resistance of a gutter layer also remains a persistent challenge. Even when selective layers achieve record-high permeabilities, module performance can be limited by the permeance of the silicone gutter layer. Highly permeable alternatives such as ultrathin poly(1-trimethylsilyl-1-propyne) (PTMSP) layers, fluorosilicones, or microporous gutter polymers have been proposed to reduce this bottleneck but require further stability improvements.

Hybrid membrane–solvent and membrane–PSA systems represent an increasingly attractive direction for deployment. In many cases, membranes can be used to pre-enrich CO_2 or remove bulk impurities, reducing the load on downstream processes. This hybridization allows membranes to operate in optimal permeability–selectivity windows while mitigating limitations related to completeness of separation.

Beyond process integration, a rigorous evaluation of material stability against contaminants such as SO_x, NO_x, and H_2S is essential, as these species may dictate the actual lifespan of membranes in industrial streams.[117,118] While laboratory-scale studies are often limited by toxicity and safety constraints, several field tests and industrial demonstrations serve as a critical validation ground. Pilot-scale trials for flue gas capture (*e.g.*, MTR (USA) and CO2CRC (Australia)) have shown that advanced polymeric modules can maintain structural integrity and separation performance even in the presence of trace SO_x and NO_x.[119–122] Notably, in the case of H_2S, membrane stability is well-established in commercial sour gas separation (*i.e.*, $H_2S/CO_2/CH_4$ mixtures), where polymeric materials have demonstrated long-term robustness even under demanding high-pressure conditions.[123,124] These practical records suggest that while degradation risks exist, they can be effectively managed

through judicious material selection and integrated process engineering.

5.4. Economic and regulatory factors

The economic landscape surrounding membrane-based CO_2 separation is shaped by a complex interplay of energy consumption, capital investment, operational stability, and regulatory incentives. Although membranes offer inherent advantages such as modularity, small footprint, and the absence of regeneration heat duty, their commercial viability depends critically on how these attributes translate into system-level costs under real operating conditions. Energy efficiency is a central consideration. For moderate CO_2 concentrations—such as those encountered in natural gas processing or biogas upgrading—membranes can outperform solvent systems by avoiding the high thermal requirements associated with solvent regeneration. However, for dilute post-combustion flue gas streams, the low partial pressure of CO_2 necessitates either high membrane permeance or multi-stage configurations with vacuum operation, both of which influence cost. Achieving permeance values exceeding 1000 GPU in robust, thin-film composite architectures is therefore a primary requirement for membranes to achieve parity with amine scrubbing in large-scale power and industrial facilities.[12,13]

To provide a clearer economic benchmark for industrial viability, it is essential to compare membrane performance against incumbent technologies using quantitative techno-economic analysis (TEA) metrics, specifically the cost per tonne of CO_2 captured (*i.e.*, USD per tCO_2).

In natural gas sweetening (CO_2/CH_4 separation), membranes are the established cost-leader for high-pressure feeds (greater than 50 bar). TEA studies indicate that membrane systems can achieve capture costs in the range of 15 to 25 USD per tCO_2, which is significantly lower than amine scrubbing units (typically 25 to 40 USD per tCO_2). This economic advantage is driven by the lack of feed compression requirements and the compact footprint of membrane skids, which drastically reduces capital expenditure in offshore or remote gas fields.[125]

In post-combustion CO_2 capture (CO_2/N_2 separation), low-pressure flue gas remains a challenging target; however, the gap is closing. While mature amine scrubbing processes generally operate at 60 to 80 USD per tCO_2, recent large-scale pilot data suggest that optimized multi-stage membrane systems (such as Polaris Gen-2) are approaching a target range of 40 to 55 USD per tCO_2.[12,13] By achieving energy specific consumptions below 400 kWh per tCO_2 (*versus* greater than 450 kWh per tCO_2 for amines), membranes are becoming a viable alternative for industrial sites lacking excess steam for solvent regeneration.

In blue hydrogen production (H_2/CO_2 separation), the economics currently favor hybrid approaches. While the baseline cost for carbon dioxide capture from Steam Methane Reforming (SMR) *via* amine or PSA is approximately 50 to 70 USD per tCO_2, standalone high-purity membrane units can exceed 80 USD per tCO_2 due to expensive materials like palladium.[126] Therefore, the economic sweet spot for polymeric membranes lies in bulk CO_2 capture from high-pressure syngas to reduce the load on downstream PSA units, rather than acting as a standalone purification stage.

Finally, for biogas upgrading (CO_2/CH_4 separation), membranes have effectively displaced water scrubbing and PSA in many new installations. Recent economic assessments place the membrane capture cost at 42 to 50 USD per tCO_2.[127,128] This is highly competitive with, and often superior to, amine scrubbing (50 to 70 USD per tCO_2) at the small-to-medium scales typical of agricultural digesters, where the economies of scale for solvent columns are diminished by high fixed costs.

In addition to the capture cost, operational stability also plays a decisive economic role. High-free-volume polymers, although capable of exceptional intrinsic transport, are susceptible to physical aging, swelling, or plasticization, all of which diminish performance over time. Frequent module replacement or accelerated performance decay increases operational expenditure, undermining the cost advantage of membrane systems. Materials such as TR polymers and PIMs offer improved resistance to these degradation mechanisms, but their long-term behavior in industrially relevant thin-film formats remains an open question. Feed-gas pretreatment further contributes to cost. Removing particulates, SO_x, NO_x, H_2S, or heavy hydrocarbons is often necessary to prevent membrane deterioration, and the associated auxiliary equipment can rival or exceed the capital cost of the membrane unit itself.

In this context, regulatory frameworks and carbon policies exert a profound influence on membrane competitiveness. Carbon pricing, tax credits such as the U.S. 45Q incentive,[129] emissions-trading schemes, and renewable gas mandates directly shape the economic attractiveness of CO_2 capture and upgrading technologies. Biogas markets provide a particularly illustrative example: strong policy support in Europe and North America has made membrane systems the default choice for upgrading CO_2-rich biogas streams into biomethane, because modular deployment and simple operation align well with distributed biogas infrastructure. Conversely, uncertainty in long-term carbon pricing or regulatory enforcement can delay investment in membrane systems for post-combustion capture or industrial decarbonization. Thus, economic and regulatory factors determine not only whether membranes can compete with incumbent technologies, but also which membrane materials are likely to advance from laboratory demonstration to full-scale implementation.

5.5. Opportunities and strategic challenges

The rapidly evolving energy and industrial landscape presents significant opportunities for polymeric CO_2 separation membranes, yet these opportunities are coupled with substantive challenges that must be addressed for widespread adoption. One of the most promising avenues lies in the development of advanced materials that exhibit exceptional resistance to plasticization and aging, particularly under high-pressure or CO_2-rich environments. TR polymers and PIMs demonstrate the potential to maintain strong selectivity and high permeance under harsh conditions that would rapidly degrade conventional polymers such as CA and PSf. As natural gas fields

become sourer and hydrogen hubs expand, demand for membranes capable of withstanding aggressive feeds is expected to rise, providing a fertile application space for these next-generation materials.

Hybrid process configurations offer another promising frontier. Integrating membranes with solvent-based absorption or PSA systems allows each technology to operate under optimized conditions, improving overall efficiency. Membranes can be used, for example, to remove bulk CO_2 upstream of a solvent unit, reducing regeneration energy, or to polish PSA off-gas streams, enhancing hydrogen recovery. These hybrid architectures reduce system-wide energy consumption and offer flexibility for retrofitting existing industrial plants, broadening the use cases for polymeric membranes. Moreover, as digitalization permeates industrial operations, membrane systems stand to benefit from advances in sensor integration, predictive maintenance, automated fault detection, and optimization algorithms. These tools can reduce downtime, lower operating costs, and provide real-time control over membrane performance—attributes that strengthen the business case for modular, distributed CO_2 separation systems.

Despite these opportunities, several challenges continue to inhibit large-scale membrane deployment. Thin-film stability is among the most persistent. While TR polymers and advanced PIM derivatives offer exceptional intrinsic performance, translating these properties into submicrometer selective layers remains challenging due to brittleness, defect formation, and accelerated aging in ultrathin geometries. Scaling these materials into hollow-fiber formats compounds the difficulty, as mechanical stresses during spinning can induce microdefects or delamination. As a result, many high-performance materials remain confined to laboratory-scale flat-sheet tests, highlighting the need for new fabrication techniques, defect-healing strategies, and improved gutter-layer designs that reduce resistance without compromising durability.

Standardization represents another major barrier. Unlike mature separation technologies, gas separation membranes lack universally accepted protocols for lifetime testing, chemical resistance evaluation, and performance certification. Differences in testing conditions across laboratories complicate comparisons between materials and impede commercialization. Establishing standardized methods for evaluating CO_2 permeance, plasticization onset, and long-term stability under realistic mixed-gas conditions would greatly accelerate industrial adoption.

Finally, regulatory uncertainty poses a systemic challenge. Markets in which membranes show strong technical potential—such as post-combustion CO_2 capture or blue hydrogen production—are heavily influenced by policy incentives, carbon pricing schemes, and emissions mandates. Fluctuating regulatory environments can disincentivize early adoption of new membrane technologies, even when performance is promising. Ensuring stable, long-term policy frameworks is therefore essential for membrane-based CO_2 capture to achieve widespread deployment.

Taken together, these opportunities and challenges underscore the central thesis of this review: that the future of polymeric membranes for CO_2 separation hinges not only on materials innovation, but on the integration of chemistry, thin-film engineering, module design, and industrial economics. Advances in polymer architecture must be accompanied by strategies for scalable fabrication, robust long-term performance, and alignment with emerging decarbonization markets. The convergence of these factors will determine how—and how rapidly—the membrane industry transitions into its next phase of technological and commercial growth.

6. Future directions and conclusions

The rapid evolution of polymeric membranes for CO_2 separation reflects a broader shift in the global energy and industrial landscape, where decarbonization efforts, hydrogen market expansion, and demand for modular purification systems are reshaping technological priorities. The materials innovations described in this review—spanning TR polymers, PIMs, and ether-rich CO_2-philic systems—demonstrate that substantial progress has been made toward overcoming long-standing permeability–selectivity trade-offs and stability limitations. Yet, the next decade will require not only further advances in intrinsic material performance but also deeper integration of polymer chemistry with thin-film engineering, scalable fabrication, and application-specific process design.

A central future direction involves closing the persistent gap between dense-film properties and thin-film performance. As shown across multiple high-free-volume polymer families, intrinsic permeability and selectivity do not necessarily translate into operational permeance when selective layers are reduced to submicrometer thicknesses. This disparity arises from a combination of interfacial resistance, defect susceptibility, brittleness, gutter-layer limitations, and accelerated physical aging. Moving forward, the most impactful innovations are likely to occur at the intersection of polymer design and thin-film processing. Techniques such as controlled solvent evaporation, surface-energy tuning, and additive-assisted coating can reduce defect formation and improve layer uniformity. Emerging approaches, including polymer–gutter co-continuous architectures or nanoscopic interpenetrating networks, offer promising routes to minimize interfacial resistance and unlock the full potential of ultrapermeable polymers.

Future research should also focus on stabilizing free volume and suppressing plasticization in high-free-volume materials without sacrificing permeability. Crosslinking strategies are particularly promising in this regard: covalent crosslinks can immobilize segments prone to relaxation or swelling, while dynamic or supramolecular crosslinks may enable adaptable, self-healing behavior. For example, TR polymers benefit from inherent structural rigidity, but their brittleness in ultrathin layers suggests a need for controlled crosslinking or hybridization with more flexible backbones. Similarly, PIMs and CANAL polymers show exceptional intrinsic microporosity but can undergo rapid densification in thin films; crosslinking, thermal annealing, and bulky substituent incorporation represent

practical strategies to mitigate these effects. Exploring the use of nanoporogens or porogenic additives during polymerization may also enable controlled creation of stable microporosity with reduced aging propensity.

In parallel, solubility-driven polymers—such as PEO-based systems, PDXLA, and Pebax—offer opportunities for designing membranes with strong CO_2 affinity and enhanced tolerance to humid or contaminated feeds. These materials are particularly well suited to post-combustion and biogas applications, where their humidity compatibility and ease of thin-film fabrication provide advantages over more rigid polymer systems. Future work may focus on developing ether-rich polymers with higher glass transition temperatures, reduced swelling, and tailored CO_2 interactions. Incorporating ether functionalities into rigid or semi-rigid backbones represents a promising hybrid design philosophy, merging the best attributes of solubility-selective and diffusivity-selective mechanisms.

Another future direction lies in rational materials–process co-design. Membrane performance targets should be driven by application-specific requirements rather than by a general pursuit of extreme permeability or selectivity. For instance, post-combustion capture demands exceptionally high CO_2 permeance to achieve competitive economics, whereas natural gas sweetening requires strong resistance to CO_2-induced plasticization and stable CO_2/CH_4 selectivity at high pressures. Biogas upgrading benefits from humidity-tolerant membranes with moderate selectivity but robust operational stability. These diverse constraints underscore the need for materials optimized not only for intrinsic transport but also for their roles within larger process flowsheets, including hybrid systems. Process modeling and TEA should therefore play a more prominent role in guiding polymer development, helping researchers identify realistic sweet spots in permeability–selectivity space for each separation task.

Digitalization and data-driven optimization represent emerging pathways for membrane advancement. Integration of real-time monitoring, predictive maintenance algorithms, and artificial intelligence (AI)-driven performance diagnostics can extend module lifetimes and reduce operational uncertainty. Machine-learning tools may also accelerate the discovery of new polymers by predicting structure–property relationships, stability trends, and optimal fabrication parameters.[130,131] Coupling computational polymer design with high-throughput synthesis and characterization workflows could significantly shorten the development cycle for next-generation membrane materials, enabling faster transitions from laboratory demonstration to pilot-scale modules.

The practical utility of these digital tools is increasingly evident in recent breakthrough studies. For instance, Yang *et al.* established an interpretable ML framework trained on experimental data to directly link polymer chemistry to the permeabilities of gases such as CO_2, N_2, and CH_4.[131] By screening a vast chemical space of over 9 million hypothetical polymers, they identified thousands of candidates exceeding current Robeson upper bounds. These predictions were further validated *via* high-fidelity molecular dynamics (MD) simulations, which correlated ML-derived insights with physical parameters like fractional free volume and gas solubility distributions. Beyond property prediction, the field is now transitioning toward AI-guided structural optimization. Cao *et al.* recently demonstrated how "explainable AI (XAI)" can deconvolute the intricate relationships between monomer architecture and transport properties.[132] This approach enables the precise design of membrane structures with targeted pore sizes and chemical affinities, effectively shortening the development cycle from laboratory demonstration to industrial application.

Scalability and manufacturability remain pivotal challenges. Many promising polymers, particularly TR and PIM derivatives, have yet to be integrated into commercial hollow-fiber spinning processes due to brittleness, solubility limitations, or poor film-forming behavior. Collaborative research between polymer chemists, membrane manufacturers, and process engineers will be essential to develop new spinning dope formulations, controlled coagulation strategies, and composite fiber architectures that can accommodate high-rigidity materials. At the same time, further innovation in gutter-layer materials with significantly higher permeability could unlock order-of-magnitude increases in module-level performance, enabling ultrathin selective layers to achieve permeances predicted by intrinsic polymer properties.

Policy and regulatory stability will also shape the future of membrane deployment. Although carbon pricing, tax incentives, and emissions standards can dramatically improve membrane competitiveness, fluctuations in policy frameworks remain a barrier to large-scale investment. Clear long-term decarbonization pathways—such as commitments to blue hydrogen infrastructure or enforceable carbon capture mandates—would spur investment in membrane technologies and accelerate their adoption across industrial sectors. Membrane suppliers and system integrators must therefore align their strategies with evolving regulatory environments and anticipate regional differences in market maturity.

Ultimately, the advancement of polymeric membranes for CO_2 separation will depend on a synergistic integration of molecular-level innovation, thin-film engineering, scalable fabrication, and system-level optimization. The materials surveyed in this review illustrate the breadth of strategies available to overcome permeability–selectivity trade-offs and address key challenges such as aging, plasticization, and process compatibility. Yet, no single polymer class will dominate all CO_2 separation scenarios. Rather, the future will be shaped by a portfolio of membrane materials, each tailored to specific feed conditions, process requirements, and economic constraints.

In conclusion, polymeric CO_2 separation membranes are poised to play a transformative role in decarbonization, hydrogen purification, and distributed gas processing. Continued progress will require a holistic approach that aligns materials science with engineering pragmatism and economic realism. By integrating advances in polymer architecture with scalable membrane fabrication and application-driven process design, the membrane community can unlock the full potential of polymeric materials as versatile, energy-efficient tools for a

low-carbon future. The convergence of high-performance polymers, optimized TFC structures, and intelligent process integration suggests that the next decade may mark a decisive turning point in the industrial deployment of membrane-based CO_2 separation technologies.

Author contributions

Prof. T. H. Lee and B. K. Lee equally contributed to this work; they were responsible for the conceptualization, data curation, and the original draft preparation. Dr Y. H. Cho participated in the technical discussion and formal analysis of TR polymers, while Prof. H. W. Kim contributed to the critical review of PIM-based materials and coordinated funding acquisition. Dr S. H. Han and Dr S. Y. Ha provided expert insights and analysis regarding the techno-economic aspects and industrial implementation of membrane systems. Prof. H. B. Park served as the corresponding author and was responsible for the overall supervision, project administration, and final editing of the manuscript.

Conflicts of interest

There are no conflicts to declare.

Data availability

No primary research results, software or code have been included and no new data were generated or analysed as part of this review.

Acknowledgements

This work was supported by the Alchemist Project funded by the Korea Evaluation Institute of Industrial Technology (Alchemist Project, NTIS-2410013669, 20018940) through the Ministry of Trade, Industry and Energy, Korea. This work was also supported by the National Research Foundation of Korea (NRF) grant funded by the Korea government (MSIT) (No. RS-2023-00254645).

References

1 IEA, Net Zero Emissions by 2050.
2 Y. Yan, T. N. Borhani, S. G. Subraveti, K. N. Pai, V. Prasad, A. Rajendran, P. Nkulikiyinka, J. O. Asibor, Z. Zhang, D. Shao, L. Wang, W. Zhang, Y. Yan, W. Ampomah, J. You, M. Wang, E. J. Anthony, V. Manovic and P. T. Clough, *Energy Environ. Sci.*, 2021, **14**, 6122–6157.
3 C. Hepburn, E. Adlen, J. Beddington, E. A. Carter, S. Fuss, N. Mac Dowell, J. C. Minx, P. Smith and C. K. Williams, *Nature*, 2019, **575**, 87–97.
4 M. K. Mondal, H. K. Balsora and P. Varshney, *Energy*, 2012, **46**, 431–441.
5 R. Stuart Haszeldine, *Science*, 2009, **325**, 1647–1652.
6 C. Song, Q. Liu, S. Deng, H. Li and Y. Kitamura, *Renewable Sustainable Energy Rev.*, 2019, 265–278.
7 L. Riboldi and O. Bolland, *Energy Procedia*, 2017, **114**, 2390–2400.
8 M. Galizia, W. S. Chi, Z. P. Smith, T. C. Merkel, R. W. Baker and B. D. Freeman, *Macromolecules*, 2017, **50**, 7809–7843.
9 H. B. Park, J. Kamcev, L. M. Robeson, M. Elimelech and B. D. Freeman, *Science*, 2017, **356**, eaab0530.
10 R. W. Baker and K. Lokhandwala, *Ind. Eng. Chem. Res.*, 2008, **47**, 2109–2121.
11 R. W. Baker and B. T. Low, *Macromolecules*, 2014, **47**, 6999–7013.
12 T. C. Merkel, H. Lin, X. Wei and R. Baker, *J. Membr. Sci.*, 2010, **359**, 126–139.
13 T. Merkel, R. Baker, P. Hao, J. Kniep, Z. He, Y. (Ivy) Huang and W. Salim, *J. Membr. Sci.*, 2026, **738**, 124829.
14 L. M. Robeson, *J. Membr. Sci.*, 2008, **320**, 390–400.
15 B. Comesaña-Gándara, J. Chen, C. G. Bezzu, M. Carta, I. Rose, M. C. Ferrari, E. Esposito, A. Fuoco, J. C. Jansen and N. B. McKeown, *Energy Environ. Sci.*, 2019, **12**, 2733–2740.
16 R. Swaidan, B. Ghanem and I. Pinnau, *ACS Macro Lett.*, 2015, **4**, 947–951.
17 H. B. Park, C. H. Jung, Y. M. Lee, A. J. Hill, S. J. Pas, S. T. Mudie, E. Van Wagner, B. D. Freeman and D. J. Cookson, *Science*, 2007, **318**, 254–258.
18 N. B. McKeown, *Polymer*, 2020, **202**, 122736.
19 J. Wu, F. Hillman, C. Z. Liang, Y. Jia and S. Zhang, *J. Mater. Chem. A*, 2023, **11**, 17452–17478.
20 S. Fujikawa, R. Selyanchyn and T. Kunitake, *Polym. J.*, 2020, **53**, 111–119.
21 S. Fujikawa and R. Selyanchyn, *MRS Bull.*, 2022, **47**, 416–423.
22 Y. Ding, *Ind. Eng. Chem. Res.*, 2020, **59**, 556–568.
23 S. Wang, X. Li, H. Wu, Z. Tian, Q. Xin, G. He, D. Peng, S. Chen, Y. Yin, Z. Jiang and M. D. Guiver, *Energy Environ. Sci.*, 2016, **9**, 1863–1890.
24 E. Favre, *Chem. Eng. J.*, 2011, **171**, 782–793.
25 A. Brunetti, F. Scura, G. Barbieri and E. Drioli, *J. Membr. Sci.*, 2010, **359**, 115–125.
26 J. G. Wijmans and R. W. Baker, *J. Membr. Sci.*, 1995, **107**, 1–21.
27 M. Omidvar, H. Nguyen, J. Liu and H. Lin, *Curr. Opin. Chem. Eng.*, 2018, **20**, 50–59.
28 K. Mizrahi Rodriguez, W. N. Wu, T. Alebrahim, Y. Cao, B. D. Freeman, D. Harrigan, M. Jhalaria, A. Kratochvil, S. Kumar, W. H. Lee, Y. M. Lee, H. Lin, J. M. Richardson, Q. Song, B. Sundell, R. Thür, I. Vankelecom, A. Wang, L. Wang, C. Wiscount and Z. P. Smith, *J. Membr. Sci.*, 2022, **659**, 120746.
29 T. H. Lee and Z. P. Smith, *Nat. Mater.*, 2024, **23**, 11–12.
30 M. Liu, M. D. Nothling, S. Zhang, Q. Fu and G. G. Qiao, *Prog. Polym. Sci.*, 2022, **126**, 101504.
31 M. Liu, M. D. Nothling, P. A. Webley, Q. Fu and G. G. Qiao, *Acc. Chem. Res.*, 2019, **52**, 1905–1914.
32 M. Liu, K. Xie, M. D. Nothling, P. A. Gurr, S. S. L. Tan, Q. Fu, P. A. Webley and G. G. Qiao, *ACS Nano*, 2018, **12**, 11591–11599.

33 M. S. Seong, H. J. Lee, A. Randová, K. Friess and J. S. Lee, *Chem. Eng. J.*, 2025, **522**, 167335.
34 L. M. Robeson, *J. Membr. Sci.*, 1991, **62**, 165–185.
35 B. D. Freeman, *Macromolecules*, 1999, **32**, 375–380.
36 K. Mizrahi Rodriguez, F. M. Benedetti, N. Roy, A. X. Wu and Z. P. Smith, *J. Mater. Chem. A*, 2021, **9**, 23631–23642.
37 Z. X. Low, P. M. Budd, N. B. McKeown and D. A. Patterson, *Chem. Rev.*, 2018, **118**, 5871–5911.
38 H. B. Park, S. H. Han, C. H. Jung, Y. M. Lee and A. J. Hill, *J. Membr. Sci.*, 2010, **359**, 11–24.
39 Q. Liu, D. R. Paul and B. D. Freeman, *Polymer*, 2016, **82**, 378–391.
40 S. H. Han, H. J. Kwon, K. Y. Kim, J. G. Seong, C. H. Park, S. Kim, C. M. Doherty, A. W. Thornton, A. J. Hill, E. Lozano, K. A. Berchtold and Y. M. Lee, *Phys. Chem. Chem. Phys.*, 2012, **14**, 4365–4373.
41 X. Hu, W. H. Lee, J. Y. Bae, J. S. Kim, J. T. Jung, H. H. Wang, H. J. Park and Y. M. Lee, *J. Membr. Sci.*, 2020, **612**, 118437.
42 J. Lee, J. S. Kim, J. F. Kim, H. J. Jo, H. Park, J. G. Seong and Y. M. Lee, *J. Membr. Sci.*, 2019, **573**, 393–402.
43 B. Comesaña-Gándara, M. Calle, H. J. Jo, A. Hernández, J. G. de la Campa, J. de Abajo, A. E. Lozano and Y. M. Lee, *J. Membr. Sci.*, 2014, **450**, 369–379.
44 Q. Liu, H. Borjigin, D. R. Paul, J. S. Riffle, J. E. McGrath and B. D. Freeman, *J. Membr. Sci.*, 2016, **518**, 88–99.
45 S. Kim, J. Hou, Y. Wang, R. Ou, G. P. Simon, J. G. Seong, Y. M. Lee and H. Wang, *J. Mater. Chem. A*, 2018, **6**, 7668–7674.
46 S. Kim, S. H. Han and Y. M. Lee, *J. Membr. Sci.*, 2012, **403–404**, 169–178.
47 Q. Liu, H. Borjigin, D. R. Paul, J. S. Riffle, J. E. McGrath and B. D. Freeman, *J. Membr. Sci.*, 2016, **518**, 88–99.
48 R. Guo, D. F. Sanders, Z. P. Smith, B. D. Freeman, D. R. Paul and J. E. McGrath, *J. Mater. Chem. A*, 2013, **1**, 262–272.
49 D. F. Sanders, R. Guo, Z. P. Smith, Q. Liu, K. A. Stevens, J. E. McGrath, D. R. Paul and B. D. Freeman, *Polymer*, 2014, **55**, 1636–1647.
50 J. Geun Seong, W. Hee Lee, J. Lee, S. Young Lee, Y. Seong Do, J. Yong Bae, S. Ju Moon, C. Hoon Park, H. Jin Jo, J. Sung Kim, K.-R. Lee, W.-S. Hung, J.-Y. Lai, Y. Ren, C. J. Roos, R. P. Lively and Y. Moo Lee, *Sci. Adv.*, 2021, **7**, eabj9062.
51 W. H. Lee, J. G. Seong, J. Y. Bae, H. H. Wang, S. J. Moon, J. T. Jung, Y. S. Do, H. Kang, C. H. Park and Y. M. Lee, *J. Membr. Sci.*, 2021, **625**, 119157.
52 Y. Wang, B. S. Ghanem, Z. Ali, K. Hazazi, Y. Han and I. Pinnau, *Small Struct.*, 2021, **2**, 2100049.
53 P. M. Budd, B. S. Ghanem, S. Makhseed, N. B. McKeown, K. J. Msayib and C. E. Tattershall, *Chem. Commun.*, 2004, 230–231.
54 R. Swaidan, B. Ghanem, E. Litwiller and I. Pinnau, *Macromolecules*, 2015, **48**, 6553–6561.
55 K. Mizrahi Rodriguez, S. Lin, A. X. Wu, K. R. Storme, T. Joo, A. F. Grosz, N. Roy, D. Syar, F. M. Benedetti and Z. P. Smith, *Chem. Soc. Rev.*, 2024, **53**, 2435–2529.
56 C. G. Bezzu, M. Carta, A. Tonkins, J. C. Jansen, P. Bernardo, F. Bazzarelli and N. B. Mckeown, *Adv. Mater.*, 2012, **24**, 5930–5933.
57 B. S. Ghanem, R. Swaidan, E. Litwiller and I. Pinnau, *Adv. Mater.*, 2014, **26**, 3688–3692.
58 X. Ma, Z. Zhu, W. Shi, W. Ji, J. Li, Y. Wang and I. Pinnau, *J. Mater. Chem. A*, 2021, **9**, 5404–5414.
59 R. Swaidan, B. Ghanem, M. Al-Saeedi, E. Litwiller and I. Pinnau, *Macromolecules*, 2014, **47**, 7453–7462.
60 I. Rose, M. Carta, R. Malpass-Evans, M. C. Ferrari, P. Bernardo, G. Clarizia, J. C. Jansen and N. B. McKeown, *ACS Macro Lett.*, 2015, **4**, 912–915.
61 I. Rose, C. G. Bezzu, M. Carta, B. Comesanã-Gándara, E. Lasseuguette, M. C. Ferrari, P. Bernardo, G. Clarizia, A. Fuoco, J. C. Jansen, K. E. Hart, T. P. Liyana-Arachchi, C. M. Colina and N. B. McKeown, *Nat. Mater.*, 2017, **16**, 932–937.
62 M. Carta, M. Croad, R. Malpass-Evans, J. C. Jansen, P. Bernardo, G. Clarizia, K. Friess, M. Lanč and N. B. McKeown, *Adv. Mater.*, 2014, **26**, 3526–3531.
63 J. Chen, M. Longo, A. Fuoco, E. Esposito, M. Monteleone, B. Comesaña Gándara, J. Carolus Jansen and N. B. McKeown, *Angew. Chem., Int. Ed.*, 2023, **62**, e202215250.
64 M. Carta, M. Croad, J. C. Jansen, P. Bernardo, G. Clarizia and N. B. McKeown, *Polym. Chem.*, 2014, **5**, 5255–5261.
65 M. Carta, R. Malpass-Evans, M. Croad, Y. Rogan, M. Lee, I. Rose and N. B. McKeown, *Polym. Chem.*, 2014, **5**, 5267–5272.
66 M. Carta, R. Malpass-Evans, M. Croad, Y. Rogan, J. C. Jansen, P. Bernardo, F. Bazzarelli and N. B. McKeown, *Science*, 2013, **339**, 303–307.
67 M. D. Guiver and Y. M. Lee, *Science*, 2013, **339**, 284–285.
68 H. W. H. Lai, F. M. Benedetti, Z. Jin, Y. C. Teo, A. X. Wu, M. G. De Angelis, Z. P. Smith and Y. Xia, *Macromolecules*, 2019, **52**, 6294–6302.
69 H. W. H. Lai, F. M. Benedetti, J. M. Ahn, A. M. Robinson, Y. Wang, I. Pinnau, Z. P. Smith and Y. Xia, *Science*, 2022, **375**, 1390–1392.
70 N. R. Horn and D. R. Paul, *Polymer*, 2011, **52**, 1619–1627.
71 R. R. Tiwari, J. Jin, B. D. Freeman and D. R. Paul, *J. Membr. Sci.*, 2017, **537**, 362–371.
72 W. F. Yong, K. H. A. Kwek, K. S. Liao and T. S. Chung, *Polymer*, 2015, **77**, 377–386.
73 M. Alberto, R. Bhavsar, J. M. Luque-Alled, A. Vijayaraghavan, P. M. Budd and P. Gorgojo, *J. Membr. Sci.*, 2018, **563**, 513–520.
74 M. Liu, X. Lu, M. D. Nothling, C. M. Doherty, L. Zu, J. N. Hart, P. A. Webley, J. Jin, Q. Fu and G. G. Qiao, *ACS Mater. Lett.*, 2020, **2**, 993–998.
75 K. Mizrahi Rodriguez, A. X. Wu, Q. Qian, G. Han, S. Lin, F. M. Benedetti, H. Lee, W. S. Chi, C. M. Doherty and Z. P. Smith, *Macromolecules*, 2020, **53**, 6220–6234.
76 S. Yi, B. Ghanem, Y. Liu, I. Pinnau and W. J. Koros, *Sci. Adv.*, 2019, **5**, eaaw5459.
77 N. Du, H. B. Park, G. P. Robertson, M. M. Dal-Cin, T. Visser, L. Scoles and M. D. Guiver, *Nat. Mater.*, 2011, **10**, 372–375.

78 C. R. Mason, L. Maynard-Atem, N. M. Al-Harbi, P. M. Budd, P. Bernardo, F. Bazzarelli, G. Clarizia and J. C. Jansen, *Macromolecules*, 2011, **44**, 6471–6479.
79 T. H. Lee, T. Joo, P. Jean-Baptiste, P. A. Dean, J. Y. Yeo and Z. P. Smith, *J. Mater. Chem. A*, 2024, **12**, 24519–24529.
80 S. Wongwilawan, T. S. Nguyen, T. P. N. Nguyen, A. Alhaji, W. Lim, Y. Hong, J. S. Park, M. Atilhan, B. J. Kim, M. Eddaoudi and C. T. Yavuz, *Nat. Commun.*, 2023, **14**, 2096.
81 T. H. Lee, P. A. Dean, J. Y. Yeo and Z. P. Smith, *Adv. Mater.*, 2026, **38**, e13892.
82 H. Lin and B. D. Freeman, *J. Membr. Sci.*, 2004, **239**, 105–117.
83 J. Liu, S. Zhang, D. Jiang, C. M. Doherty, A. J. Hill, C. Cheng, H. B. Park and H. Lin, *Joule*, 2019, **3**, 1881–1894.
84 J. H. Kim, Y. Ha and Y. M. Lee, *J. Membr. Sci.*, 2001, **190**, 179–193.
85 J. Liu, X. Hou, H. B. Park and H. Lin, *Chem. – Eur. J.*, 2016, **22**, 15980–15990.
86 C. E. Powell and G. G. Qiao, *J. Membr. Sci.*, 2006, **279**, 1–49.
87 L. Huang, W. Guo, H. Mondal, S. Schaefer, T. N. Tran, S. Fan, Y. Ding and H. Lin, *Macromolecules*, 2022, **55**, 382–389.
88 H. Lin and B. D. Freeman, *Macromolecules*, 2006, **39**, 3568–3580.
89 H. Lin, E. Van Wagner, J. S. Swinnea, B. D. Freeman, S. J. Pas, A. J. Hill, S. Kalakkunnath and D. S. Kalika, *J. Membr. Sci.*, 2006, **276**, 145–161.
90 H. Lin, E. V. Wagner, B. D. Freeman and R. P. Gupta, *Science*, 2006, **311**, 639–642.
91 H. Lin, T. Kai, B. D. Freeman, S. Kalakkunnath and D. S. Kalika, *Macromolecules*, 2005, **38**, 8381–8393.
92 G. Zhang, S. Dong, N. Esmaeili, F. Attia, K. Chen, F. Pazanialenjareghi and H. Lin, *Small*, 2025, **21**, 2503461.
93 V. I. Bondar, B. D. Freeman and I. Pinnau, *J. Polym. Sci., Part B:Polym. Phys.*, 1999, **37**, 2463–2475.
94 V. I. Bondar, B. D. Freeman and I. Pinnau, *J. Polym. Sci., Part B:Polym. Phys.*, 2000, **38**, 2051–2062.
95 W. Yave, A. Car and K. V. Peinemann, *J. Membr. Sci.*, 2010, **350**, 124–129.
96 A. Car, C. Stropnik, W. Yave and K. V. Peinemann, *J. Membr. Sci.*, 2008, **307**, 88–95.
97 J. Wei, M. Deng, Z. Qin, W. Zhao, Y. Li, R. Selyanchyn, H. Zhao, J. Dong, D. Yin, Y. Zhuang, L. Deng, L. Yang, L. Yao, W. Jiang, J. Zheng, B. Van der Bruggen and Z. Dai, *Adv. Sci.*, 2025, **12**, 2501330.
98 F. H. Akhtar, M. Kumar and K. V. Peinemann, *J. Membr. Sci.*, 2017, **525**, 187–194.
99 Y. Li, Q. Xin, H. Wu, R. Guo, Z. Tian, Y. Liu, S. Wang, G. He, F. Pan and Z. Jiang, *Energy Environ. Sci.*, 2014, **7**, 1489–1499.
100 O. Selyanchyn, R. Selyanchyn and S. Fujikawa, *ACS Appl. Mater. Interfaces*, 2020, **12**, 33196–33209.
101 T. H. Lee, figshare, 2026, DOI: 10.6084/m9.figshare.31165048.
102 K. Xie, Q. Fu, G. G. Qiao and P. A. Webley, *J. Membr. Sci.*, 2019, **572**, 38–60.
103 W. Ogieglo, G. Genduso, J. Rubner, J. H. P. de Vaumas, M. Wessling and I. Pinnau, *Macromolecules*, 2020, **53**, 8765–8774.
104 W. Ogieglo, B. Ghanem, X. Ma, M. Wessling and I. Pinnau, *ACS Appl. Mater. Interfaces*, 2018, **10**, 11369–11376.
105 M. Yu, A. B. Foster, M. Alshurafa, J. M. Luque-Alled, P. Gorgojo, S. E. Kentish, C. A. Scholes and P. M. Budd, *J. Membr. Sci.*, 2023, **679**, 121697.
106 S. Harms, K. Rätzke, F. Faupel, N. Chaukura, P. M. Budd, W. Egger and L. Ravelli, *J. Adhes.*, 2012, **88**, 608–619.
107 T. H. Lee, M. Balçık, B. K. Lee, B. S. Ghanem, I. Pinnau and H. B. Park, *J. Membr. Sci.*, 2023, **672**, 121438.
108 M. Yu, A. B. Foster, C. A. Scholes, S. E. Kentish and P. M. Budd, *ACS Macro Lett.*, 2023, **12**, 113–117.
109 O. Selyanchyn, R. Selyanchyn and S. Fujikawa, *ACS Appl. Mater. Interfaces*, 2020, **12**, 33196–33209.
110 G. L. Jadav, V. K. Aswal, H. Bhatt, J. C. Chaudhari and P. S. Singh, *J. Membr. Sci.*, 2012, **415–416**, 624–634.
111 M. Liu, M. D. Nothling, S. Zhang, Q. Fu and G. G. Qiao, *Prog. Polym. Sci.*, 2022, **126**, 101504.
112 H. Nguyen, M. Y. Hsiao, K. Nagai and H. Lin, *Polymer*, 2020, **205**, 122790.
113 H. Wang, J. K. Keum, A. Hiltner, E. Baer, B. D. Freeman, A. Rozanski and A. Galeski, *Science*, 2009, **323**, 757–760.
114 H. Nguyen, M. Wang, M. Y. Hsiao, K. Nagai, Y. Ding and H. Lin, *J. Membr. Sci.*, 2019, **586**, 7–14.
115 T. H. Lee, J. K. Jang, B. K. Lee, W. N. Wu, Z. P. Smith and H. B. Park, *Macromolecules*, 2024, **57**, 11242–11250.
116 IEA, *Global Hydrogen Review 2023*, 2023.
117 D. Damiani, J. T. Litynski, H. G. McIlvried, D. M. Vikara and R. D. Srivastava, *Greenhouse Gases: Sci. Technol.*, 2012, **2**, 9–16.
118 M. B. Hägg, A. Lindbråthen, X. He, S. G. Nodeland and T. Cantero, *Energy Procedia*, 2017, **114**, 6150–6165.
119 S. H. Choi, J. H. Kim and Y. Lee, *Sep. Purif. Technol.*, 2013, **110**, 170–180.
120 T. Merkel, J. Kniep, X. Wei, T. Carlisle, S. White, S. Pande, D. Fulton, R. Watson, T. Hoffman, B. Freeman and R. Baker, *Pilot Testing of a Membrane System for Post-Combustion CO_2 Capture Final Report*, 2010.
121 T. Merkel, W. Salim, C. Casillas, A. Borsaly, J. Kniep, E. Westling, T. Hofmann, Z. Sun, B. Boudreaux, J. Deng and J. He, *Scale-Up Testing of Advanced Polaris Membrane CO_2 Capture Technology Final Project Report*, 2023.
122 L. Deng, A. A. Lindbråthen, S. Janakiram, L. Ansalonc and Z. Dai, *Carbon Capture Sci. Technol.*, 2024, **11**, 100193.
123 Y. Ma, H. Guo, R. Selyanchyn, B. Wang, L. Deng, Z. Dai and X. Jiang, *J. Mater. Chem. A*, 2021, **9**, 23628–23638.
124 T. Joo, Y. Wu, T. H. Lee, P. A. Dean, W. N. Wu, T. M. Swager and Z. P. Smith, *J. Mater. Chem. A*, 2025, **13**, 5707–5722.
125 R. Abejón, C. Casado-Coterillo and A. Garea, *Ind. Eng. Chem. Res.*, 2022, **61**, 8149–8165.
126 D. N. H. A. Pg Haji Omar Ali, H. Suhaimi and P. E. Abas, *Hydrogen*, 2025, **6**, 9.

127 S. J. Kim, Y. Song, M. Binns, J. G. Yeo and J. K. Kim, *J. Membr. Sci.*, 2025, **713**, 123286.
128 R. Swinbourn, C. Li and F. Wang, *ChemSusChem*, 2024, **17**, e202400779.
129 J. L. Fan, M. Xu, L. Yang, X. Zhang and F. Li, *Energy Policy*, 2019, **132**, 1229–1240.
130 J. Wang, K. Tian, D. Li, M. Chen, X. Feng, Y. Zhang, Y. Wang and B. Van der Bruggen, *Sep. Purif. Technol.*, 2023, **313**, 123493.
131 J. Yang, L. Tao, J. He, J. R. McCutcheon and Y. Li, *Sci. Adv.*, 2022, **8**, eabn9545.
132 Z. Cao, O. B. Farimani, J. Ock and A. B. Farimani, *Nano Lett.*, 2024, **24**, 2953–2960.